processes

MDPI

Article

Optimal Geomechanical Parameter Selection for Enhanced ROP Modeling: A Systematic Field-Based Comparative Study

Ahmed S. Alhalboosi, Musaed N. J. AlAwad, Faisal S. Altawati, Mohammed A. Khamis * and Mohammed A. Almobarky

Department of Petroleum and Natural Gas Engineering, College of Engineering, King Saud University, Riyadh P.O. Box 800, Saudi Arabia; malawwad@ksu.edu.sa (M.N.J.A.)
* Correspondence: mokhamis@ksu.edu.sa

Abstract

Accurate prediction of Rate of Penetration (*ROP*) in carbonate formations remains constrained by the arbitrary selection of geomechanical input parameters in empirical drilling models. This study presents the first systematic field-based evaluation of sixteen geomechanical properties—grouped into three categories: strength parameters (uniaxial compressive strength (*UCS*), confined compressive strength (*CCS*), shear strength, thick-walled cylinder strength (*TWC*), friction angle, and cohesion), elastic moduli (Young's modulus, shear modulus, bulk modulus, bulk compressibility, dynamic combined modulus (*DCM*), Poisson's ratio, brittleness index), and in situ stress parameters (overburden pressure, minimum, and maximum horizontal stresses)—to identify optimal predictors for ROP modeling across PDC bit sizes of 12.25″ and 8.5″. Continuous wireline log data from two vertical carbonate wells in the Middle East (Well A: 1000–3370 m; Well B: 1945 to 3128 m; total intervals of 2370 m and 1183 m, respectively) penetrating formations comprising limestone, dolomite, sandstone, shale, anhydrite, and marly limestone were used. All sixteen geomechanical properties were computed using Interactive Petrophysics (IP) software with lithology-specific empirical correlations and validated against laboratory core measurements (R^2 = 0.79–0.95). Pearson and Spearman correlation analyses quantified parameter–*ROP* relationships, and the Al-Abduljabbar empirical model, recalibrated via multiple nonlinear regression, served as the evaluation framework. *DCM* consistently exhibited the strongest negative correlation with ROP across both bit sizes and achieved the highest model accuracy (R^2 = 0.54, AAPE = 25.33%), significantly outperforming the Bourgoyne and Young model (R^2 = 0.26, AAPE = 36.55%). A statistically validated scale-dependent effect was identified: Fisher's Z-transformation tests confirmed that the correlation reversal between *CCS* and *UCS* across bit sizes is statistically significant (*CCS*: Z = −16.84, $p < 0.001$; *UCS*: Z = −6.75, $p < 0.001$), establishing *CCS* as the superior predictor at 12.25″ and *UCS* as the superior predictor at 8.5″—a finding not previously reported in the ROP literature. This reversal is attributed to the larger contact area of the 12.25″ bit, which promotes confinement-dominated rock failure better described by *CCS*, whereas the smaller bit produces localized stress concentration better represented by *UCS*. These results establish that (1) optimal geomechanical input selection is bit-size dependent, (2) nonlinear modeling outperforms linear frameworks for strength–*ROP* relationships, and (3) parameter relevance outweighs coefficient tuning in model robustness. *DCM* is recommended as the most operationally practical universal input, requiring only conventional compressional sonic and density logs. This study provides a systematic framework for geomechanical parameter selection with direct implications for drilling optimization in heterogeneous carbonate reservoirs.

Academic Editor: Yuqiang Xu

Received: 28 March 2026
Revised: 1 May 2026
Accepted: 11 May 2026
Published: 19 May 2026

Keywords: rate of penetration (ROP); geomechanical parameters; dynamic combined modulus (*DCM*); carbonate formation; PDC bit; bit-size dependency; Fisher's Z-test; drilling optimization

1. Introduction

Rock drilling is a costly operation used in mining, petroleum, and civil and underground excavation. The drilling process is an essential task as it determines the economic success or failure of operations [1]. In this context, drilling performance assessment must be taken into account when evaluating project feasibility and economics [2].

Drilling is one of the most essential operations in the resource industry, starting from the exploration phase and continuing throughout all the stages of production process to the end of the mine life. Predicting the drillability of rocks is fundamental for efficient planning and operating of the drilling process. Several factors can affect drilling. Among these factors, the most important are the geological and mechanical properties of the formation to be drilled [3–5].

Penetration rate is an important factor for project planning and cost calculations. Estimating the drillability value affects the correct choice of drilling equipment and project cost. Drillability is influenced by many controllable and uncontrollable parameters [6].

Drillability is defined as the ability to penetrate the drill bit at a certain time in the rock. Penetration rate is the progression of the drilling bit into the rock in a certain period of time, which is generally expressed as "m/min." The penetrability of a rock can be defined in numerous ways, such as the penetration rate of the drill bit and the specific energy spent in the drilling operation. Drillability and penetration rate can be considered as similar terms. While the drillability indicates whether the penetration is easy or hard, the penetration rate indicates whether it is fast or slow [7].

Knowledge of rock's behavior helps in planning efficient drilling operations. The more accurate information available during site investigation, the more efficient the prediction of potential challenges during project implementation [8].

Geomechanics properties have been successfully applied to overcome drilling problems and improve efficiency in the petroleum industry by evaluating mechanical behavior of reservoir rock through mechanical earth models (MEMs) [9,10].

The mechanical properties of rocks are important in drilling operations such as prediction of fracture zone, wellbore stability, and other drilling engineering aspects [11].

An accurate estimation of the drilling rate (*ROP*) helps to make the planning of the rock excavation (well drilling) projects more effective. The drillability of the rocks is mainly based on operational variables and rock characteristics. Operational variables known as the controllable parameters are rotational speed (*RPM*), thrust (weight-on-bit, *WOB*), blow frequency, and flushing (mud circulation rate). Rock properties, in situ stresses, and geological conditions are the uncontrollable characteristics Kahraman et al. [12].

The operational parameters include the drilling method, bit types and shapes, and the technical aspects of the drilling rig used. The geotechnical parameters influence the drilling performance and the wear of bits and include the condition and structure of rock mass and mechanical behavior and mineral composition of rock materials (rock strength). Therefore, when evaluating a rock mass from the perspective of its penetrability, qualitative and quantitative effects of the most important drilling parameters must be examined [13].

A fundamental yet unresolved challenge in rate of penetration (ROP) modeling is the arbitrary and inconsistent selection of geomechanical input parameters. Despite decades of research spanning theoretical, statistical, empirical, and AI-driven approaches, no prior

study has systematically compared the predictive value of all available geomechanical parameters or investigated whether the optimal parameter changes with bit size. The following review section documents this gap across the literature evolution of ROP models.

Many researchers have examined the penetration rate relationship with rock properties. Cunningham [14], Walker et al. [15], and Warren [16,17] were the first to experimentally prove that the ROP depends on the *WOB*, *RPM*, compressive strength, and pore pressure, among other parameters. Warren [17] proposed a torque model and validated it using laboratory experiments and field data. The Warren's model included bit hydraulic, fluid type, and formation type. These early approaches, however, did not explicitly consider what we presently know as rock strength (e.g., unconfined compressive strength (*UCS*) and confined compressive strength (*CCS*)) and were rather focused on the formation properties [18].

Al-Betairi et al. [19] introduced a model where multiple regression analysis was applied to adjust the drilling parameters based on formation properties. The model addressed optimum *ROP*, *WOB*, and *RPM*. By considering Warren's formula, Hareland and Hoberock [20] presented an equation for predicting the *ROP* based on the *CCS*, in situ stress, *WOB*, and *RPM*.

Pandey et al. [21] investigated the correlation between penetration rate values obtained from micro-bit drilling tests and compressive strength, tensile strength, and shear strength, and the Protodyakonov strength index was found to be a logarithmic relationship. Altindag [22] demonstrated that the penetration rate was closely related to rock brittleness. Bilgin and Kahraman [23] correlated the *UCS*, point load strength, Schmidt hammer (SH) value, and Cerchar hardness. Kahraman, Bilgin, and Feridunoglu [12] carried out a detailed investigation of the rock properties affecting penetration rate of percussive drills. In their study, they correlated penetration rate to rock properties and found *UCS*, tensile strength, point load strength, and Schmidt hammer values to be the dominant rock properties for penetration rates of percussive drills. Judzis et al. [24] performed a full-scale test at bottom-hole pressure (>10,000 psi), and the results revealed the effect of *CCS* on the Polycrystalline Diamond Compact (PDC) and roller-cone bits. Yenice et al. [25] correlated drilling rate index (DRI) with mechanical rock properties of marble samples and determined a strong connection between DRI and *UCS*, tensile strength, and specific destruction energy. Prasad [26] focused on the rock mechanical properties and changed different drilling parameters to analyze their effects on the ROP. Their study results showed that the largest impacts were those of *UCS* and tensile strength of the rock and the *WOB*. Yaşar et al. [27] conducted a laboratory study on cement mortar samples to investigate the influence of operational parameters on rock drillability. The authors observed strong correlations between penetration rates, specific energies, and *UCS*s of the samples. Cheniany, Hasan, Shahriar, and Khademi Hamidi [6] proposed a model called the Specific Rock Mass Drillability (SRMD) index for predicting the penetration rate of rotary drills. They correlated SRMD with various rock properties and concluded *UCS* and SH values as the most significant factors. Yarali and Soyer [28] Examined the relationship between the DRI and various rock properties and found a decrease in linear relationships between the DRI and *UCS*, SH, Shore scleroscope hardness, and point load strength. Li et al. [29] investigated the correlation between rock drillability and mechanical properties under various pressure conditions to improve drilling safety and efficiency. The study measured compressive strength, elastic modulus, and Poisson's ratio under uniaxial (0 MPa), 30 MPa, and 60 MPa confining pressures. They utilized Rollow's microbit technique to obtain drillability numbers and then conducted a regression analysis. The researchers observed that the correlation between drillability grade (DG) and rock mechanical properties increased as confining pressure increased. The best correlation was between DG and compressive

strength under varying confined pressures, compared to the correlation between DG and elastic modulus or Poisson's ratio under uniaxial conditions. Li et al. [30] studied the impact of horizontal and vertical stresses on a PDC cutter that was superior to that of horizontal stress, as they studied the effects of vertical and horizontal stresses. Kolapo [31] examined the effect of rock mechanical properties on drilling performance using samples from Abuja, Nigeria. Point load tests were used to estimate the *UCS* and tensile strength, which were then correlated with penetration rate and specific energy. The study concluded that penetration rate decreases as *UCS* and tensile strength increase, while specific energy increases with increasing rock strength. The author also stated that pre-existing fractures in granite reduced strength, enhancing drillability, and reducing energy demand. Delavar, Ramezanzadeh, and Tokhmechi [18] studied the intricate correlations between geomechanical properties of rock and drilling parameters in carbonate reservoirs. They used advanced artificial intelligence methods (a Bayesian Network with the K2 algorithm and a Multilayer Perceptron (MLP) Artificial Neural Network) to examine the relationship between geomechanical properties such as *UCS*, internal friction angle, and vertical effective stress with drilling parameters such as rate of penetration (*ROP*), (*WOB*), and torque using a 1-D geomechanical model. Their results confirmed that *UCS* directly affects ROP, but they stated that the internal friction angle and vertically effective stress have a major impact on *WOB* and torque. The study ultimately allocated ideal ranges for adjustable drilling parameters (*WOB* and *TRQ*) in relation to rock characteristics in order to improve drilling effectiveness in the formations studied. The history of research on predicting the rate of penetration (ROP) has seen significant evolution, which can be categorized into three main stages, each addressing the limitations of the preceding one.

As shortcomings in several initial studies, many conventional ROP prediction models did not adequately account for or completely neglected the geomechanical properties of rock formation being drilled. These models were mainly focused on operational parameters (weight on bit, rotational speed, etc.), resulting in a low level of accuracy that was highly sensitive to changes in formation rock type such as the models developed by Graham and Muench [32], Galle and Woods [33], Bingham [34], Eckel [35], and Bourgoyne and Young [36].

In recent years, artificial intelligence (AI) and machine learning (ML) models emerged to overcome the non-linear complexity of the ROP prediction problem, enabling the achievement of correlations with better accuracy than those developed from traditional models. However, the challenge of geomechanical input parameters dispersion persisted and continued to influence performance. Researchers using AI and ML also demonstrated various approaches regarding the primary geomechanical input parameters. Some fed the model with (*UCS*), others used (*CCS*), elastic properties, or other combined coefficients. This persistent inconsistency and dispersion in the selection of input geomechanics variables remains the primary reason for the observed fluctuation in the accuracy of even the most advanced AI and ML models for ROP predictions. This highlights a crucial need to identify and validate the most influential and effectiveness of geomechanical input parameters for accurate ROP prediction such as models of Jahanbakhshi et al. [37], Ahmed et al. [38], Lawal et al. [39], Shaker and Hadi [40], Jiao et al. [41], and Huang et al. [42].

1.1. Limitations of the Previous Models

Table 1 presents a comprehensive review of the variation in geomechanical parameter selection across published ROP prediction models. A systematic review of the most prominent studies establishes that no previous study systematically compared geomechanical parameters to identify the optimal input for ROP prediction. Instead, researchers have

selected parameters arbitrarily—ranging from *UCS* alone to complex combinations of elastic properties and stress parameters—without comparative justification or systematic evaluation.

Table 1. Comprehensive review of ROP prediction models and their geomechanical input parameters.

Study Category	Representative Studies (n)	Geomechanics Parameter(s) Used	Critical Limitation
Theoretical Models	Maurer [43], Hareland and Rampersad [44]	*UCS*, *CCS*	Never validated against *CCS*, elastic properties, or alternatives No bit size considered in parameter selection
Statistical Models	Bourgoyne and Young [36]	None (drilling parameters only)	No geomechanical parameters included
Analytical Models (Single Parameter)	Warren [45], Hareland and Hoberock [20], Deng et al. [46]	*UCS*, *CCS*, Dynamic strength	Cannot claim optimality without testing *UCS*, elastic modulus, *DCM*, or other candidates No bit size considered in parameter selection
Empirical Models (Convention-Based)	Motahhari et al. [47], Cheniany, Hasan, Shahriar and Khademi Hamidi [6], Al-AbdulJabbar et al. [48]	*UCS*	Perpetuates potentially suboptimal parameter selection No bit size considered in parameter selection, Al-Abduljabbar used "8.5–12.25″ bits but did not validate parameter across sizes
Experimental	Judzis, Bland, Curry, Black, Robertson, Meiners and Grant [24], Li, Ling and Pu [30]	*CCS*, Horizontal and vertical stress effects	Perpetuates potentially suboptimal parameter selection No bit size considered in parameter selection
Laboratory Studies	Altindag [22], Kahraman, Bilgin and Feridunoglu [12], Bilgin and Kahraman [23], Li, Yang, Meng, Liu, Han, Zhou and Zhang [29]	*UCS*, tensile, point load, Schmidt hammer, Brittleness index, Compressive strength, elastic modulus, Poisson's ratio	Tested multiple parameters but at microbit scale; lab correlations do not transfer to field; scale effects completely ignored
AI/ML Models (Algorithm-Selected)	Jahanbakhshi, Keshavarzi and Jafarnezhad [37], Ahmed, Adeniran and Samsuri [38], Delavar, Ramezanzadeh and Tokhmechi [18], Mohammadi Behboud et al. [49], Delavar and Ramezanzadeh [50], Saad et al. [51]	Maximum horizontal stress, minimum horizontal stress, vertical stress, *UCS*, Young's modulus, cohesion, Poisson's ratio, friction angle	Algorithm-selected without physics justification; bit size effect ignored in parameter ranking
This Study	2026	Systematically tested 16 parameters: *UCS*, *CCS*, *DCM*, E_{DYN}, K_{DYN}, BC_{DYN}, *pr*, *BI*, *j*, Cohesion, *TWC*, Shear Strength, *OBP*, *SHMINP*, *SHMMAX*.	The current study is limited to two vertical carbonate wells from a single Middle East field; generalizability to other basins, lithologies, or bit types (e.g., roller-cone) is not established.

Models are classified by their foundational methodology: theoretical models derive ROP from first-principles physics (e.g., crater-formation theory); statistical models derive ROP from multi-variate regression on operational data without physical derivation; analytical models apply mechanics-based solutions for specific bit–rock interactions; AI/ML models use data-driven algorithmic feature selection.

As is evident from Table 1, parameter selection has been fundamentally arbitrary where most of studies defaulted to use *UCS* without comparative justification. Others relied on theoretical assumptions that barely validated against alternatives. Other researchers used AI algorithms to select features in a black-box manner while Saad, Taman, Reda, Yehia, Keshinro, Meehan, and Okoroafor [51] attempted systematic comparison, but tested only stress vs. drilling-only parameters, missing *UCS*, *CCS*, and *DCM*. More significantly, none of the previous studies consider whether optimal geomechanical input parameters change along with bit diameter. Even Al-AbdulJabbar, Elkatatny, Mahmoud, Abdelgawad, and Al-Majed [48], whose dataset has 8.5″ to 12.25″ PDC bits, did not validate whether *UCS* remained optimal across this range of bit sizes.

According to latest ROP modeling research, many critical gaps limit the accuracy of the predictions of these studies. This marked a significant step, aiming to improve predictive correlations accuracy by linking drilling performance directly to rock strength. However, these models suffered from inconsistent mechanical input parameters. Some studies relied heavily on (*UCS*), while others utilized confined compressive strength (*CCS*), rock elastic properties, or other specific rock strength indices. This alteration in the choice of key geomechanical input variables resulted in a fluctuation in prediction accuracy, which prevented these models from attaining the desired level of robust reliability.

Furthermore, recent studies that investigated correlations between rock geomechanics properties and ROP have largely depended on microbit laboratory experiments, which fail to capture scale effects, heterogeneous lithology, and actual downhole conditions encountered in field operations across different bit sizes.

Additionally, none of the studies cited above investigate whether the strength of correlations between geomechanical parameters and ROP varies with bit size, despite evidence that bit-rock contact area and interaction volume fundamentally influence which rock properties dominate drilling resistance.

1.2. Study Objectives

The main objective of this study is to evaluate sixteen geomechanical properties derived from the well-log data obtained from two vertical wells with different lithologies in same field. This can be done by identifying these geomechanical properties of drilled rock with actual ROP data at different PDC bit sizes. This will allow for the identification of which parameters possess the highest correlation with ROP, which parameters have highest correlation with ROP at different bits size, and which can be easy to calculate, thus providing a useful input for future predictive ROP models.

2. Methodology

This study employed an integrated approach that combined wireline log-derived geomechanical properties with a modified empirical drilling model to evaluate the impact of in situ rock mechanics on rate of penetration (ROP). Field data from two vertical wells in a carbonate reservoir in the Middle East were used to analyze the performance of PDC bits across both the 12.25″ and 8.5″ hole sections in order to determine the best predictors for drilling efficiency.

To fulfill the objective of this study, the Al-Abduljabbar model was selected as the base empirical framework because it is specifically designed to integrate multiple geomechanical

inputs and offers the flexibility to be modified for evaluating individual parameter importance. This model was then run sixteen times, each iteration incorporating a different single geomechanical property as the sole input, while all other parameters remained constant. This modified framework serves as a comparative testing environment for evaluating the predictive accuracy of each of the 16 geomechanical parameters separately. In addition, the study compares the modified model to well-known models such as Maurer [43] the statistical Bourgoyne and Young [36] model, and the original Al-Abduljabbar [48] model. This comparison aims to demonstrate the effectiveness of the modified strategy, as well as to quantify the significant gains in accuracy made by incorporating specific, high-resolution geomechanical variables—such as dynamic combined modulus—that were conspicuously missing from formulations like Bourgoyne and Young [36]. This study aims to identify the parameter that optimally balances predictive accuracy and computational efficiency for use in future rate of penetration (ROP) models.

2.1. Data Collection and Description

This research utilizes the following information:

1. This research utilizes data from two vertical wells (Well A and Well B) located in the same carbonate oil field in the Middle East. Well A covers a depth interval from 1000 to 3370 m (total drilled interval: 2370 m), while Well B covers a depth interval from 1945.5 to 3110.5 m (total drilled interval: 1183). Both wells penetrate a sequence of carbonate and mixed-siliciclastic formations comprising from the top of the drilled intervals downward: dolomite, limestone, sandstone, shale, anhydrite, and marly limestone (LS marl). The lithological column for each well was established through integration of mud logging cuttings descriptions and petrophysical well log analysis (neutron-density and sonic-neutron cross plots) as described in Section 2.2. The stratigraphic ages of the penetrated formations are consistent with Middle Cretaceous to Jurassic sequences typical of the Arabian Platform; however, precise formation names and ages are withheld for confidentiality. Various real-time sensors collect critical drilling variables to enable real-time forecasting of the rate of penetration (ROP). Drilling speed sensors monitor the rate at which the drill bit penetrates the formation (ROP), providing a real-time indication of drilling progress.
2. Operational data including weight on bit (*WOB*), rotary speed (*RPM*), torque (*TRQ*) and bit size (BS) are available.
3. Well log sensors measure the physical characteristics of the formation, such as gamma rays log (GR), density log (RHOB), neutron log (TNPH), PEF log, compressional and shear sonic log (DTCM and DTSM), Spontaneous Potential log (SP), caliper log, formation temperature log, and deep resistivity log (DR).
4. Drilling fluid properties including mudflow sensors continuously monitor the flow rate of the drilling, mud weight (MW) and standpipe pressure (SPP), ensuring borehole cleanliness and preventing issues like wall collapse or stuck drill bits.

Detailed information on all parameters for Well A is provided in Table 2.

Table 2. Statistical analysis of the dataset of Well A.

	Min	Max	SD	Mean	P10	P50	P90
TVD (m)	1000	3370.1	684.2	2185	1237	2185	3133.1
ROP (m/hr)	1.9	92.7	10.7	19.6	8.81	17.3	33.3
SPP (psi)	1023.6	2540	257.6	1931.5	1647.7	1882	2327.3
FLOWPUMPS (L/m)	1091.9	3078.9	571.2	2278.1	1802	1843.3	3014.8
WOB (ton)	0.1	18.9	2.8	7.4	4.4	7	11.6
Torque (Ibf-ft)	944.5	21,686.5	3072.5	9139.2	5938.9	8633.3	13,668.7

Table 2. *Cont.*

	Min	Max	SD	Mean	P10	P50	P90
RPM	93.7	286	57.9	198.9	132	224	257
BS (in)	8.5	12.25	1.8	10	8.5	8.5	12.2
GR (API)	0.3	182	22.6	36.3	15.6	30.4	67.9
RHOB (g/cc)	1.3	2.9	0.1	2.4	2.2	2.4	2.6
NEUTRON	−0.026	0.7	0.1	0.2	0.06	0.17	0.39
CALIPAR (in)	6	24.8	2.3	10.3	8.1	9.7	12.3
DTSM (us/ft)	62.8	421.2	28.1	139.8	110.3	135.7	173.4
DTCM (us/ft)	41	167.4	11.8	73.9	60.3	73	89.1
PEF	1.6	9.4	1.02	3.8	2.3	3.6	4.9
SP	−58	43.3	24.9	−1.2	−31.3	6.6	26.1
RD (ohm-meters)	0.18	1449.5	4.4	3.6	0.7	2.7	26.5
TEMP (C)	56	80.1	6.9	68	58.4	68	77.7

2.2. Rock Geomechanical Properties

The relationship between drilling parameters, geomechanical characteristics, and rate of penetration (ROP) is complicated, with each element having a unique impact on drilling effectiveness. The behavior of rocks under stress is governed by geomechanical characteristics such as Poisson's ratio (*pr*), Young's modulus (E_{DYN}), dynamic combined modulus (*DCM*), and confined compressive strength (*CCS*), which have a direct impact on ROP through bit performance and energy. These characteristics are often calculated from well logs using empirical correlations (e.g., between bulk density and seismic wave velocities). For this study, The IP software 2018 (developed and commercialized by Geoactive Ltd., Aberdeen, UK) was used to estimate all these properties from the available log data. This software can calculate these properties using empirical correlations specifically for each rock type, which gives much more accurate results. The lithology column of two wells was carried out through an incorporated approach, combining mud logging data and petrophysical well log analysis. Mud logging data descriptions, documented cuttings, gas readings, and lithological features of drilled rock were analyzed across all well intervals to provide preliminary lithological classifications. To refine and validate these interpretations depth accuracy, Neutron-density, and sonic-Neutron cross plots are used for each section as shown in Figure 1. Based on these analyses, a lithology column is formed, which is essential for geomechanics rock analysis, especially for unconfined compression strength (*UCS*) and dynamic elastic properties where the IP software uses different equations to estimate it based on lithology type.

The dynamic shear modulus is calculated based on shear sonic (*DTs*) and density (RHOB) logs as shown in Equation (1), while the dynamic Poisson's ratio was calculated based on compressional (*DTc*) and shear (*DTs*) sonic logs as shown in Equation (2)

$$G_{\mathrm{DYN}} = 1.34747 \times 10^{10} \times \left(RHOB/DTs^2\right) \tag{1}$$

$$pr_{DYN} = \left(\left(\frac{1}{2}\right)\left(\frac{DTs}{DTc}\right)^2 - 1\right) \Big/ \left(\left(\frac{DTs}{DTc}\right)^2 - 1\right) \tag{2}$$

Equation (3) shows the dynamic bulk modulus, which was calculated based on density, compressional (*DTc*), and shear (*DTs*) sonic logs. On the other hand, the dynamic bulk compressibility was estimated based on elastic wave propagation theory and based on the dynamic Poisson's ratio and dynamic Young's modulus as illustrated in Equation (4).

$$K_{DYN} = 1.34747 \times 10^{10} \times RHOB\left(\frac{1}{DTc^2} - \frac{1}{3 \times DTs^2}\right) \tag{3}$$

$$BC_{DYN} = 3 * (1 - 2 * pr_{DYN}) / E_{DYN} \quad (4)$$

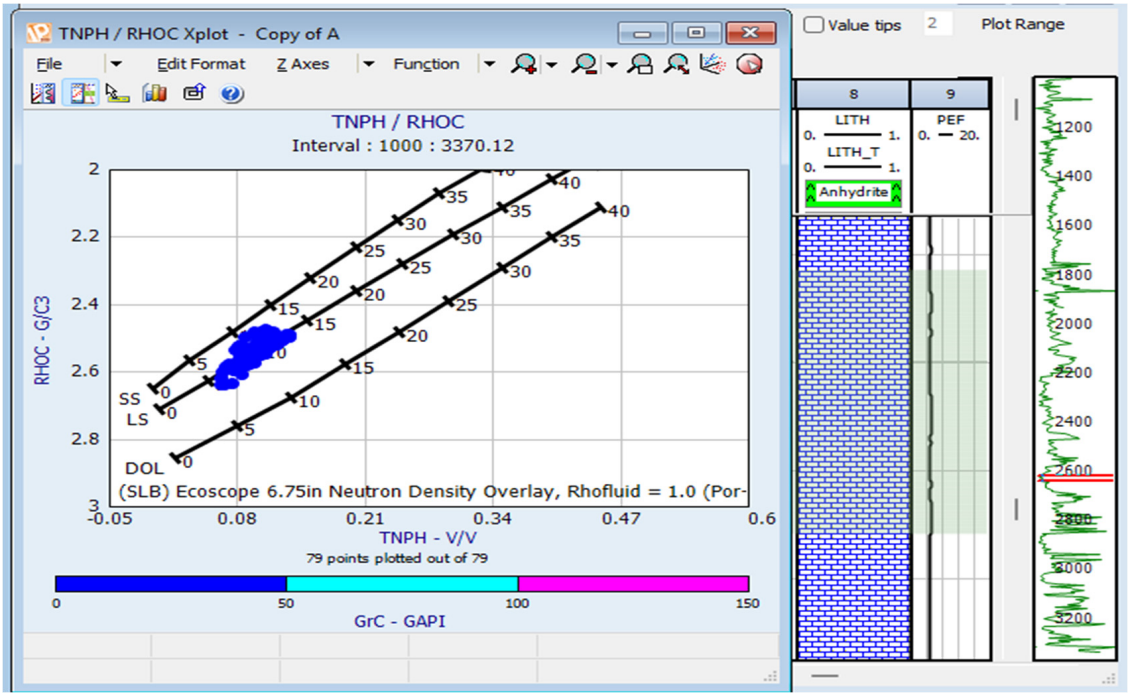

Figure 1. Cross plot of Neutron-density log generated using IP software, over lithology clusters and corresponding well depth intervals.

The dynamic Young's modulus calculated based on dynamic shear modulus and Poisson's ratio as shown in Equation (5).

$$E_{DYN} = 2 * G_{DYN} * (1 + pr_{DYN}) \quad (5)$$

The dynamic combined modulus (K_{DYN} + (4/3) G_{DYN}) is estimated based on density and compressional when shear sonic (*DTs*) is unavailable as shown in Equation (6).

$$DCM = (K_{DYN} + (\frac{4}{3})G_{DYN}) = 1.344747 \times 10^4 * (RHOB/DTc^2) \quad (6)$$

The Brittleness Index (*BI*) In this study was calculated using Equation (7), which follows the method proposed by Rickman et al. [52] and combines normalized Young's modulus and Poisson's ratio.

$$BI = \left(\frac{E_{DYN} - E_{DYNmin}}{E_{DYNmax} - E_{DYNmin}} + \frac{pr_{DYN} - pr_{DYNmax}}{pr_{DYNmin} - pr_{DYNmax}} \right) / 2 \quad (7)$$

UCS was estimated by using lithology-specific empirical models available for sandstone, shale, carbonate, and dolomite. Each well was divided into multiple zones based on lithological interpretation, and an appropriate *UCS* correlation was applied to each zone. A composite *UCS* curve was generated by combining the results from all zones, ensuring continuity across lithological boundaries. Table 3 follows the method proposed by IP software for *UCS* calculation based on lithology type, where (Φ) is the porosity.

Table 3. The equations used to estimate *UCS* in IP software.

Equation	Use of the Equation	Equation No.
$(111.5 \times e^{(-11.6 \times \Phi)} \times 145.038$	Sandstone, porosity > 30%	Equation (8)
$(43 - (140 \times \Phi) + (63 \times \Phi^2)) \times 145.038$	Sandstone, porosity range 20% to 35%	Equation (9)
$(43 - (140 \times NPHI) + (63 \times NPHI^2)) \times 145.038$	Sandstone, porosity range 20% to 35%	Equation (10)
$(140 - (2.1 \times DT) + (0.0083 \times DT^2)) \times 145.038$	Sandstone, sonic transit time range 90 to 140 µsecs/ft	Equation (11)
$(277 \times e^{(-10 \times \Phi)} \times 145.038$	Sandstone, porosity range 0.2% to 33%	Equation (12)
$(254 - 204 * VCL)(1 - 2.7\Phi)^2) \times 145.038$	Shaly sandstone, porosity < 30%	Equation (13)
$ESTA \times (0.008 \times VCL + 0.0045 \times (1 - VCL))$	Sandstone, based on static Young's modulus and clay volume	Equation (14)
$(0.43 \times (304.8/DT)^{3.2}) \times 145.038$	Shale, Pliocene, and younger rocks in the Gulf of Mexico	Equation (15)
$(1.35 \times (304.8/DT)^{2.6}) \times 145.038$	Shale, global application	Equation (16)
$(0.286 \times (\Phi - 1.762)) \times 145.038$	Shale, high porosity	Equation (17)
$(1.001 \times (\Phi - 1.143)) \times 145.038$	Shale, low porosity (typically <10%)	Equation (18)
$10 \times (304.8/DT - 1) \times 145.038$	Shale, based on sonic travel time	Equation (19)
$(0.77 \times (304.8/DT)^{2.93}) \times 145.038$	Shale, high porosity North Sea tertiary shales	Equation (20)
$(2.922 \times (\Phi - 0.96)) \times 145.038$	Shale, high porosity North Sea tertiary shales	Equation (21)
$0.0232 \times ESTA^{0.91}$	Shale, based on static Young's modulus	Equation (22)
$10(2.44 + (0.9314/DT))$	Carbonate, based on sonic travel time	Equation (23)
$143 \times e^{(-6.95 \times \Phi)} \times 145.038$	Carbonate, low to moderate porosity ($0.05 < \Phi < 0.2$), high UCS ($30 < UCS < 150$ MPa)	Equation (24)
$135.9 \times e^{(-4.8 \times \Phi)} \times 145.038$	Carbonate, low to moderate porosity ($0 < \Phi < 0.2$), high UCS ($10 < UCS < 300$ MPa)	Equation (25)
$(7682/DT)^{1.82}$	Carbonate, based on sonic travel time	Equation (26)
$40,020 \times (1 - 3 \times \Phi)^2$	Carbonate, based on porosity	Equation (27)
$64 \times ESTA^{0.34}$	Dolomite, *UCS* range 8700 psi to 14,500 psi	Equation (28)

The thick-walled cylinder tensile strength (*TWC*) which is made up of *TWC* values derived from two models. The *TWC* models covered in IP include lithology type, then the values combine into a single curve based on that type. The first one is created by upscaling the *UCS* Composite curve. The upscaling parameters can be changed, and the default values in IP are A = 80.884 and B = 0.57, which are globally applicable values for sandstones as shown in Equation (29).

$$TWC\_UCS\ Upscaler = A\ *\ UCS\ Composite^B \quad (29)$$

where *UCS* Composite: unconfined compressive strength composite across all zones in the well (psi); A and B: scaling-up factors (unitless), while the second curve is calculated based on Density and Sonic curves as shown in Equation (30).

$$TWC\_Veeken = (1.18 * \left(9.29 * 10^5 * \left(\frac{RHOB}{DTc^2}\right)\right) + 0.00226 * \left(9.29 * 10^5 * \left(\frac{RHOB}{DTc^2}\right)^2\right) * 14.5 \quad (30)$$

The friction angle (j) is determined using IP software, where software uses special formulas for each lithology type, and the composite curve is done by combination of the last formulas. Equation (31) is applicable to shales while Equation (32) is for sandstones. On the other hand, Equation (33) is applied to both sandstones and shales, where V_{clay} is clay volume and Equation (34) is applied for shale formation.

$$\mathrm{j} = \sin^{-1}\left(\left(\frac{304,878}{DT} - 1000\right)/\left(\frac{304,878}{DT} + 1000\right)\right) \tag{31}$$

$$\mathrm{j} = 57.75 - 105 * \Phi \tag{32}$$

$$\mathrm{j} = 26.5 - 37.4\left(1 - \Phi - V_{clay}\right) + 62.1\left(1 - \Phi - V_{clay}\right)^2 \tag{33}$$

$$\mathrm{j} = 11 * \left(\frac{304.8}{DT}\right) - 10.2 \tag{34}$$

The shear strength (SS) and confined compressive strength (CCS) is added to IP software, and it calculated using the Mohr–Coulomb failure criterion, where the shear strength is calculated using Equation (35).

$$SS = c + \sigma_n \tan \mathrm{j} \tag{35}$$

where σ_n is normally effective stress in (psi) and c is Rock Cohesion (psi). Then, the confined compressive strength (CCS) equation is derived from Mohr–Coulomb failure criterion as shown in Equation (36).

$$CCS = UCS + \sigma_n \times \tan^2\left(45 + \frac{\mathrm{j}}{2}\right) \tag{36}$$

Rock Cohesion (c) can be computed using Equation (37) as a function of the unconfined compressive strength (UCS) and the internal friction angle (j), as given by Jaeger et al. [15]:

$$c = \frac{UCS}{2 \times \left[\left(\sqrt{1 + (\tan \mathrm{j})^2}\right) + \tan \mathrm{j}\right]} \tag{37}$$

The overburden pressure is computed using following formula:

$$OBP = g \times \int_0^z \rho\,(D) dD \tag{38}$$

where $\rho(D)$ is density log value at depth D, and g is gravitational constant (unit-adjusted). The pore pressure of both wells was calculated in Interactive Petrophysics (IP) software using Eaton's sonic method, where the pore pressure gradient is derived from the empirical relationship:

$$\frac{PP}{D} = \frac{OBP}{D} - \left(\frac{OBP}{D} - \frac{PP_n}{D}\right) \times \left(\frac{\Delta t_{NCT}}{\Delta t_{observed}}\right)^x \tag{39}$$

where PP/D is pore pressure gradient, (psi/ft), OBP/D is overburden gradient, (psi/ft), PP_n/D is normal hydrostatic gradient (e.g., 0.465 psi/ft), Δt_{NCT} is the acoustic travel time obtained from NCTL at the depth of examination, and $\Delta t_{observed}$ is the acoustic travel time from sonic log Exponent x = taken as 3.0.

The minimum horizontal stress is calculated using Eaton [53] equation:

$$SHMINP = \frac{pr_{DYN}}{1 - pr_{DYN}}(OBP - PP) + PP \tag{40}$$

where $SHMINP$ is minimum horizontal stress (psi), OBP is overburden pressure (in psi), PP is pore pressure (in psi/ft).

The maximum horizontal stress is also calculated using the Li and Purdy [54] equation:

$$SHMMAX = \frac{(SHMINP - PP)}{pr_{DYN}} - OBP + 2 \times PP \quad (41)$$

where $SHMMAX$ is maximum horizontal stress (psi).

The data set comprises points, and the results are visually represented in their distribution and range in Figure 2.

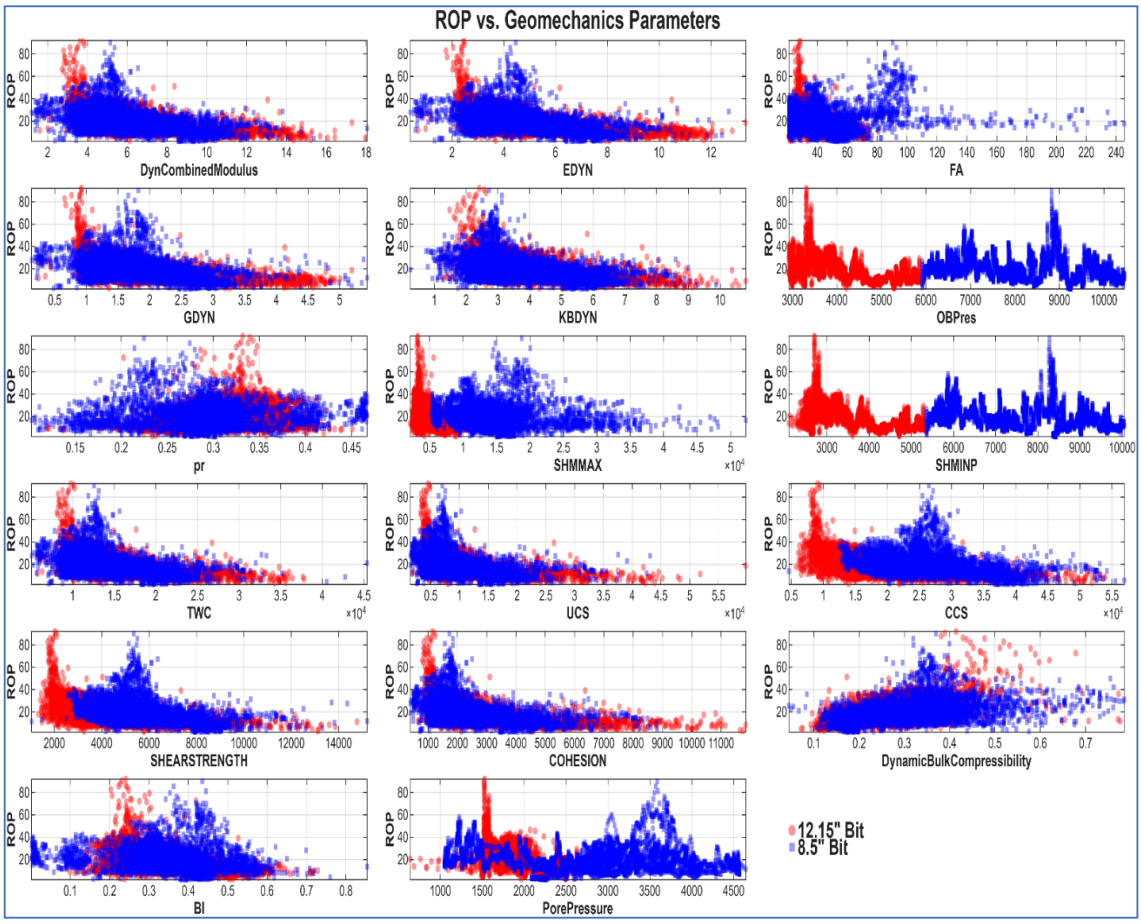

Figure 2. Scatter plot of data points investigated in this study.

2.3. Rock Mechanical Properties from Laboratory Tests

Four Laboratory tests (UCS, pr, Young's modulus, and friction angle) were conducted on core samples retrieved from Well B at depths intervals of 2140 m, 2450 m, 2730 m, and 3077 m, covering limestone, sandstone, and shale lithologies. Two types of standard geomechanical tests were performed in accordance with International Society for Rock Mechanics and Rock Engineering (ISRM) recommended procedures: Triaxial Compression Strength (TCS) tests to determine static elastic parameters and rock failure criteria, using cylindrical specimens of 1 inch diameter and 2 inches length, and Uniaxial Compressive Strength (*UCS*) tests on specimens of 10 inches diameter and 20 inches length. These static measurements serve as a benchmark for validating log-derived (dynamic) estimates at equivalent depths.

A well-documented discrepancy exists between static (lab-measured) and dynamic (log-derived) elastic parameters. Dynamic parameter values are typically higher due to

the influence of microfractures, pores, and bedding planes that are not fully captured in high-frequency sonic measurements. To enable meaningful comparison, dynamic elastic properties must be converted to their static equivalents.

In this study, only Young's modulus and Poisson's ratio required conversion. Poisson's ratio was assumed to be equivalent in both static and dynamic domains (i.e., no conversion applied). For Young's modulus, lithology-specific empirical correlations were used to transform dynamic to static values: Equation (42) for sandstone, Equation (43) for shale, and Equation (44) for mixed lithologies. These conversions were implemented in the petrophysical workflow to ensure consistency between modelled and laboratory-observed rock behavior.

$$E_{st} = 0.0293 * E_{DYN}{}^2 + 0.4533 * E_{DYN} \quad (42)$$

$$E_{st} = 0.0428 * E_{DYN}{}^2 + 0.2334 * E_{DYN} \quad (43)$$

$$E_{st} = 0.018 * E_{DYN}{}^2 + 0.422 * E_{DYN} \quad (44)$$

2.4. Correlation Analysis

The selection of features is based on a comprehensive correlation analysis in order to clarify the connection between various geomechanics rock properties and the rate of penetration (ROP). In this study, the Pearson correlation coefficient and the Spearman rank correlation coefficient help to evaluate the direction and intensity of the link between variables. The Pearson coefficient is chosen to define the linear relationship between ROP and each geomechanics variable, assuming the data follows a bivariate standard distribution. Additionally, the Spearman coefficient evaluates monotonic relationships, regardless of their linearity. This non-parametric method assigns value to the data before calculating the correlation, which helps to find nonlinear relationship that Pearson's method might fail to do.

2.5. Model Formulation

Identifying the geomechanical parameter that affects ROP calculation the most requires evaluating all sixteen parameters within the ROP model. The Maurer [43] model—one of the earliest developed for this purpose—was selected as a suitable baseline. Maurer's model postulates a perfect cleaning theory, in which ROP is governed by crater formation efficiency beneath the bit tooth. However, this model omits several influential parameters, such as torque and hydraulics.

$$ROP = K\frac{RPM * WOB^2}{BS^2 * UCS^2} \quad (45)$$

where K is the formation drillability constant, RPM is revolutions per minute, WOB is weight on bit (Ibf), BS is bit size (in), and UCS is the Uniaxial compression strength (psi). Bourgoyne and Young [36] developed a mathematical model using statistical synthesis of the old drilling data to define eight drilling parameters (x_n) and eight exponents (a_n) that require multiple regressions to calculate the best values for these constants to build a complete ROP model. However, this model ignores the rock properties effects.

$$ROP = (f_1) * (f_2) * (f_3) \ \ldots * (f_8) \quad (46)$$

in which

$$f_1 = e^{2303a_1} \quad (47)$$

$$f_2 = e^{2303a_2}(10,000 - D) \quad (48)$$

$$f_3 = e^{2303a_3 TVD^{0.69}(g_p - 9)} \tag{49}$$

$$f_4 = e^{2303a_4 TVD(g_p - ECD)} \tag{50}$$

$$f_5 = \left[\frac{\left(\frac{W}{BS}\right) - \left(\frac{W}{BS}\right)_t}{4 - \left(\frac{W}{BS}\right)_t} \right]^{a5} \tag{51}$$

$$f_6 = \left(\frac{N}{60}\right)^{a6} \tag{52}$$

$$f_7 = e^{-a_7 h} \tag{53}$$

$$f_8 = \left(\frac{F_j}{1000}\right)^{a8} \tag{54}$$

where TVD shows the true vertical depth (ft), D is depth (ft), g_p is pore pressure gradient (lbm/gal), ECD expresses the equivalent circulating density (lbf/gal), $(WOB/BS)_t$ shows the threshold bit weight per inch of bit size at which the bit begins to drill (lbf/in), h is bit tooth dullness, and F_j is the jet impact force (lbf).

The Al-Abduljabbar model [48] uses data from carbonate reservoirs in the Middle East to build this empirical model. It combined a thorough set of drilling parameters with mud properties and rock properties that are suitable for our objective as it represents the interaction of all these properties to evaluate which rock geomechanics is more effective for ROP predicting. The original formulation employs fixed exponents taken from the author's particular dataset:

$$ROP = \frac{16.96(\ WOB^a * RPM * TRQ * SPP * \ Q)}{BS^2 * UCS^b * \rho * PV} \tag{55}$$

where a and b are model coefficients and will be calculated by nonlinear regression (the authors proposed 0.85 and 1.16 for the values of these parameters, respectively), TRQ is torque (klbf-ft), Q is flow rate (gpm), PV is plastic viscosity (cp), SPP is standpipe pressure (psi), and ρ is the mud weight (pcf).

Knowing that fixed exponents sometimes fall when used to different geological formations with varying rock-bit interactions, this study suggests a modified Al-Abduljabbar Model.

This study uses Multiple Nonlinear Regression (MNR) with logarithmic linearization rather than depending on the initial coefficients (a = 0.85, b = 1.16). This statistical method optimizes the exponents for every input parameter concurrently based on the local field data, therefore allowing the model to adapt particularly to the examined formation. The modified general equation is:

$$ROP = K\frac{\left(WOB^{a1} * RPM^{a2} * TRQ^{a3} * HHP^{a4}\right)}{BS^{a5} * \rho^{a6} * \mathrm{B}^{a7} * GeoParam^{a8}} \tag{56}$$

where K is the optimized drillability constant, HHP is hydraulic horsepower, GeoParam represents the specific geomechanical parameter being tested (e.g., *UCS*, *CCS*, or dynamic combined modulus), and a1, a2, a3, . . ., a8 are the optimized exponents derived from the regression.

This method allows for a straightforward sensitivity analysis where we can statistically determine which rock property has the greatest impact on drillability by holding drilling parameters constant and changing a number of geomechanics variables.

3. Results and Discussion

3.1. Dynamic Geomechanics Result

After the lithology column has been estimated, *UCS*, pore pressure, bulk modulus, *TWC*, shear modulus, brittleness, Poisson's ratio, and other geomechanics properties were analyzed and determined against depth for the formations of the studied wells. Figure 3 shows the geomechanics properties of well A. In this study it was found that the prevailing stress state in studied field is a strike–slip faulting according to the results, where it revealed that the highest stress was the maximum horizontal stress (*SHMMAX*), then the overburden pressure (*OBP*) and the lowest was the minimum horizontal stress (*SHMINP*). The result also shows that the carbonate formation like limestone and dolomite have higher strength and elasticity than other formations like sandstone while the shale formation shows weakest strength. Furthermore, the results show that as the depth increases, the strength of formation increases due to the formation being under higher compaction in addition to the increase in the in situ stress with depth which puts the rock under higher confining stress leading to the increase in strength and elastic properties of the rock. In contrast, dynamic bulk compressibility increases in formations such as sandstone and shale while decreasing in carbonate formations. Tables 4 and 5 show the statistical properties of Wells A and B.

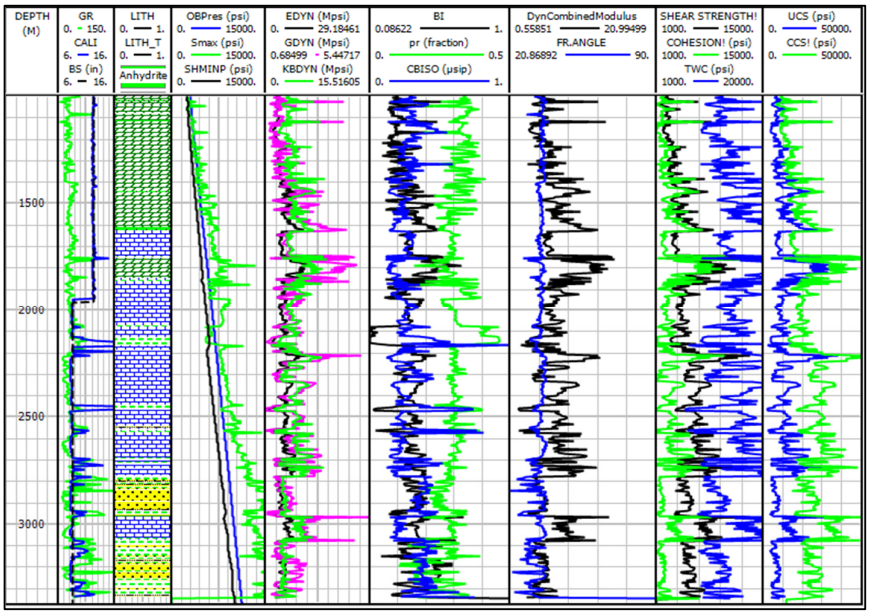

Figure 3. Geomechanics properties, BI, j, pr, EDYN, GDYN, KBDYN, dynamic bulk compressibility (CBISO) and dynamic combined modulus of Well A.

Table 4. Geomechanics properties of Well A.

	Min	Max	SD	Mean	P10	P50	P90
BI	0	0.9	0.1	0.3	0.2	0.3	0.5
CCS (psi)	4650.1	56,909.9	8640.4	23,088.4	12,289.2	22,448.4	35,025.2
COHESION (psi)	384.4	11,839	1504.7	2655.8	1256.5	2214.8	4615.6
DCM (Mpsi)	1.2	18.1	2.3	6.6	4	6.2	9.9
BC_{DYN} (µsip)	0	0.8	0.1	0.3	0.2	0.3	0.4
E_{DYN} (Mpsi)	0.4	13.3	1.9	4.9	2.8	4.6	7.5
j (degree)	20.9	245.4	19	44	25.2	40.5	61.3
G_{DYN} (Mpsi)	0.1	5.4	0.8	1.9	1	1.8	2.9
K_{DYN} (Mpsi)	0.2	10.8	1.5	4.1	2.4	3.9	6.1
OBP (psi)	2918.4	10,457	2178.2	6630.1	3638.7	6601.5	9674.1

Table 4. *Cont.*

	Min	Max	SD	Mean	P10	P50	P90
Pore Pressure (psi)	638.1	4643.7	800.4	2497.5	1552.2	2416.7	3667.6
ROP (m/hr)	1.9	92.7	10.7	19.6	8.81	17.3	33.3
SHEARSTRENGTH (psi)	1028.4	15,200	1932.2	5078.7	2752.6	4909.3	7753
SHMINP (psi)	2096	10,050.5	2167.4	5987	3027	5845.2	9052.7
SHMMAX (psi)	2071.8	52,251.4	6321.3	10,440.8	3685.4	9280.5	17,800
TWC (psi)	5056.8	45,372.6	4773	15,133.8	9933.5	14,119.9	21,458.9
UCS (psi)	1415.9	59,717.4	6060.5	10,308.6	4631	8576.1	17,905.1
pr	0.1	0.5	0.1	0.3	0.2	0.3	0.4

Table 5. Geomechanics properties of Well B.

	Min	Max	SD	Mean	P10	P50	P90
BI	0	0.6	0.1	0.3	0.3	0.3	0.4
CCS (psi)	2988.2	56,173.8	7483.8	19,874.2	10,979.4	19,229.7	30,138.5
COHESION (psi)	418.3	10,448.1	1484.5	3000.2	1481	2622.2	5152.7
DCM (Mpsi)	1.6	18.6	2.5	7.2	4.3	6.9	10.6
BC_{DYN} (µsip)	0.1	0.9	0.1	0.3	0.2	0.2	0.4
E_{DYN} (Mpsi)	1.8	11	1.6	5.2	3.2	4.9	7.6
j (degree)	20.9	51.2	6.8	37.6	27.5	38.2	46.1
G_{DYN} (Mpsi)	0.8	4.2	0.6	2	1.3	1.9	2.9
K_{DYN} (Mpsi)	0.3	13.9	1.8	4.5	2.5	4.4	6.7
OBP (psi)	5879	10,141.5	1192.6	8036.6	6375.5	8036.5	9668
Pore Pressure (psi)	359.7	7211.9	1165.2	4491.9	3097.6	4263.6	6231.1
ROP (m/hr)	1	43.8	5.1	9.6	3.4	9.1	15
SHEARSTRENGTH (psi)	473.4	12,506.5	1562.4	3252.4	1618.2	2872.9	5469.4
SHMINP (psi)	4888.5	9742.4	1108.8	7031	5378.8	7099.6	8370.6
SHMMAX (psi)	4457.2	19,162.8	2410.3	9539.5	6803.8	9064.1	13,194.7
TWC (psi)	5300.1	36,961.5	4641.4	15,887.3	10,398.2	15,227.2	22,412.2
UCS (psi)	1537.1	45,284.6	5762.5	11,159.8	5015.9	9796.6	19,294.5
pr	0.1	0.5	0	0.3	0.3	0.3	0.3

3.2. Comparison Between Data Calculated from Well-Log and from Core Test

Rock geomechanical properties validation using core-log integration demonstrates strong relationships between laboratory-derived core measures and estimated well log parameters for a variety of rock types. Routine testing of many core samples from various wellbore depths was used to get a complete geomechanical description. For all examined features, the cross-plot analysis reveals strong consistency between the core and log data. Poisson's ratio relationship is $R^2 = 0.7893$. A strong linear relationship, indicating the reliable predictive power of log-based computations for this crucial elastic characteristic, governs how rock deforms under pressure. The accuracy of the dynamic to static modulus conversions used for sonic log data is supported by the strong association observed in the Young's modulus comparison ($R^2 = 0.9511$). The Unconfined Compressive Strength (*UCS*) cross-plot also demonstrates strong association ($R^2 = 0.8683$). The Friction Angle cross-plot also demonstrates strong association ($R^2 = 0.8734$). These high correlation values for geomechanical properties validate the reliability of log-based geomechanical models and provide confidence in their usage for wellbore analysis, strategies for finishing drilling, and design. The methodical validation technique, which uses numerous core samples from different depths, ensures that formation variability is represented in the characterization and creates Robust calibration links that may be confidently used across the whole wellbore interval for comprehensive geomechanically analysis and operational decision-making. Figures 4–7 show the cross plot of tested parameters.

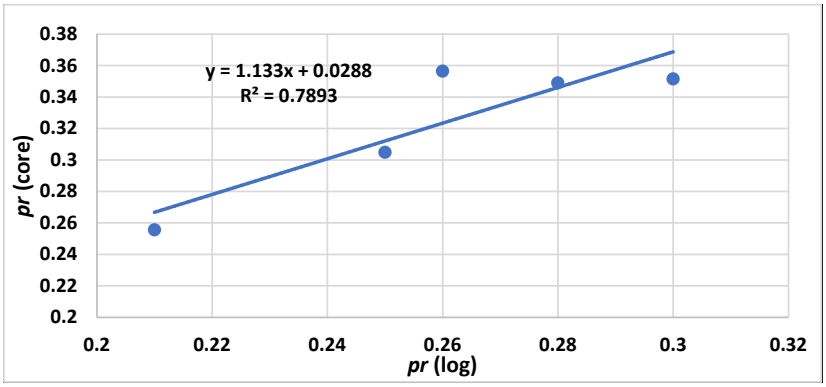

Figure 4. Cross plot for Poisson's ratio calculated from core and log.

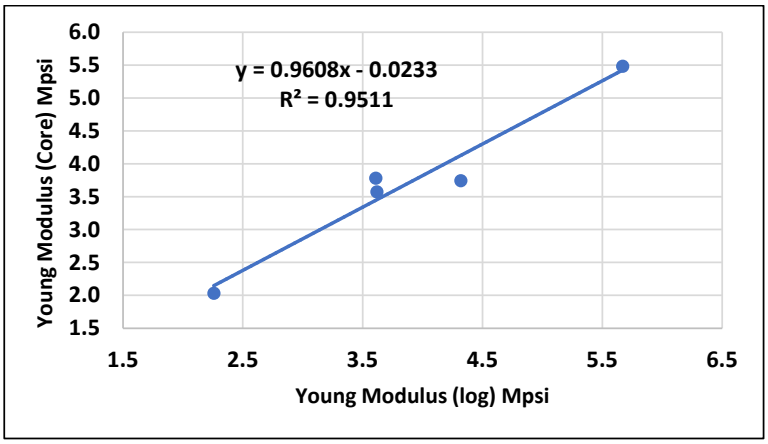

Figure 5. Cross plot for Young's modulus calculated from core and log.

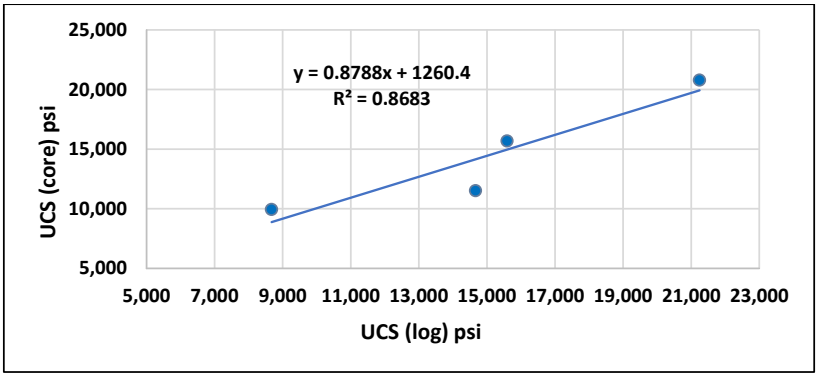

Figure 6. Cross plot for *UCS* calculated from core and log.

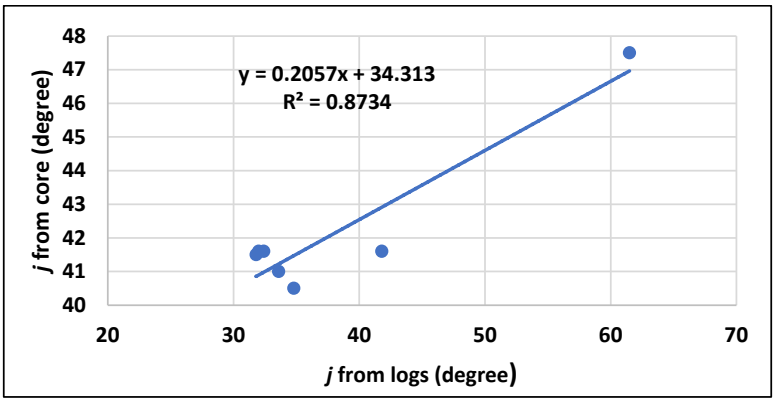

Figure 7. Cross plot friction angle calculated from core and log.

3.3. Correlation Results

A correlation analysis was conducted to determine the correlation between the rate of penetration (ROP) and an estimated sixteen rock geomechanics parameters. This research quantifies these correlations across two-bit sizes and manufactory bits made by utilizing Pearson (linear) and Spearman (monotonic) coefficients, with the findings shown in Figures 8 and 9. The 12.25″ PDC Haliburton dataset was excluded from this discussion because of its restricted depth range, which makes a representative study impossible. The most remarkable and significant correlations were observed with the 12.25″ PDC SMITH, where a very powerful negative correlation was found between ROP and variables measuring rock strength and stiffness. The highest correlation result was with shear strength (Pearson= −0.52, Spearman= −0.68), *CCS* (Pearson= −0.53, Spearman= −0.67) and dynamic combined modulus (Pearson= −0.55, Spearman= −0.63). These results confirm the fundamental idea that greater inherent strength and resistance to deformation in rocks makes drilling them more difficult.

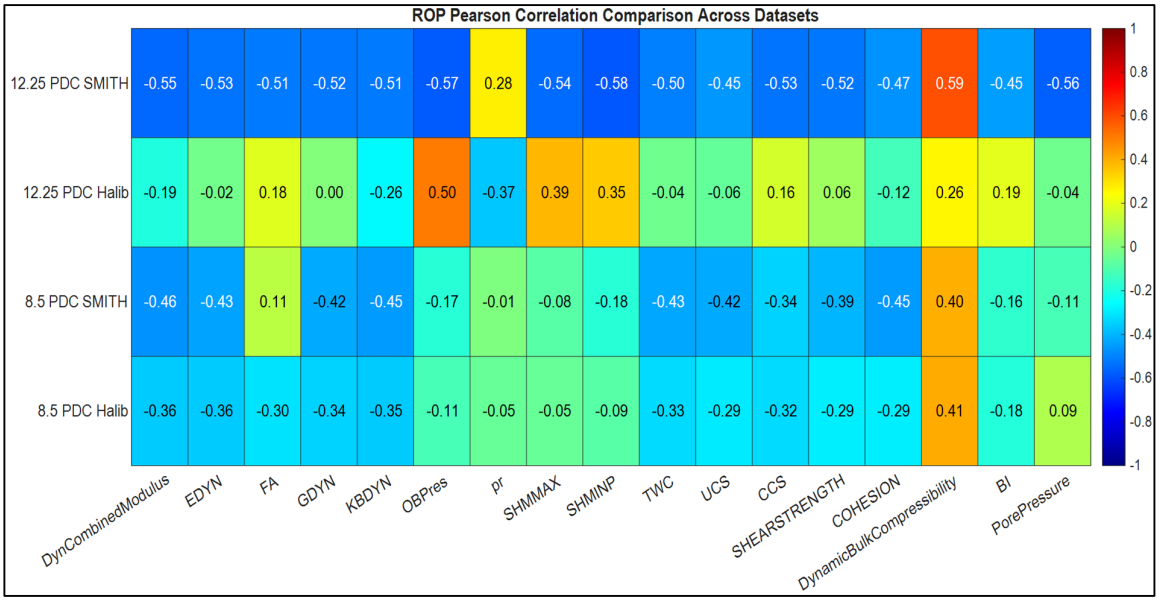

Figure 8. Pearson heatmap correlation for geomechanics properties with ROP.

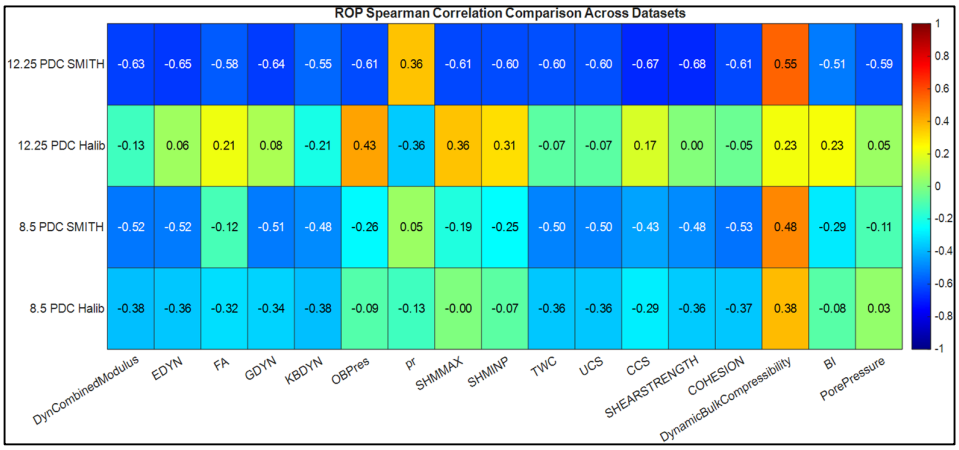

Figure 9. Spearman heatmap correlation for geomechanics properties with ROP.

In contrast, Dynamic Bulk Compressibility exhibits the strongest positive correlation (Pearson = 0.59, Spearman = 0.55) that indicate the more compressible formations, which are less resistant to volumetric change, facilitate more efficient rock failure, and increase

ROP. The correlations observed in the 8.5″ PDC-bit sizes were typically lower than those in the 12.25″ PDC-bit size, despite the fact that the overall trends remained the same.

In general, the difference in correlation strength between the 12.25″ PDC bit size and 8.5″ PDC bit size is likely due to a scale effect where the larger bit contact with a greater area of drilled rock that may make it slightly less effected with geomechanics parameter compared with larger bit size.

Furthermore, a distinct inversion in the influence of compressive strength parameters was observed when reducing the bit size. For the 12.25″ PDC SMITH configuration, *CCS* exhibited a significantly stronger correlation (Pearson= −0.53, Spearman= −0.67) compared to *UCS* (Pearson= −0.45, Spearman= −0.60). However, this trend reverses in the 8.5″ PDC SMITH section. Here, the influence of *CCS* diminishes notably (Pearson= −0.34, Spearman= −0.43), while *UCS* maintains a stronger monotonic relationship, particularly in the Spearman analysis (Pearson= −0.42, Spearman= −0.50).

Fisher's Z-transformation tests confirmed that the correlation reversal between *CCS* and *UCS* across bit sizes is statistically significant (*CCS*: $Z = -16.84$, $p < 0.001$; *UCS*: $Z = -6.75$, $p < 0.001$), establishing that *CCS* is the superior predictor at 12.25″. This reversal is physically attributed to the difference in bit-rock contact area: the larger 12.25″ bit generates a broader confinement field beneath the cutters, favoring *CCS* which accounts for confining stress via the Mohr–Coulomb criterion, whereas the smaller 8.5″ bit produces localized stress concentration beneath individual cutters with minimal bulk confinement, a failure regime more accurately represented by *UCS*.

This finding has significant implications for ROP predictive modeling: strength parameter selection must account for bit size as an essential design consideration.

Based on comparative analysis across all bit sizes, formations, and correlation methods, the dynamic combined modulus is recommended as the most robust input parameter for ROP predictive modeling. While other parameters such as Shear Strength and *CCS* exhibit high sensitivity in specific large-bit scenarios, compressive strength parameters demonstrated scale-dependent inversions (*CCS* vs. *UCS*).

The dynamic combined modulus maintained a high consistency in both Pearson and Spearman analyses across both the 12.25″ PDC bit and 8.5″ PDC bit. Its ability to represent the elastic stiffness of the rock while maintaining a linear relationship closer to that of the Spearman ideal makes it a reliable, universally applicable feature for drilling optimization models.

3.4. Selection of the Effective Geomechanics Parameter

Three of the most common models for ROP prediction—Maurer [43], Bourgoyne and Young [36], and Al-Abduljabbar [48]—were selected to compare their performance using field data from two wells drilled through heterogeneous formations. The relative performance of the models for both wells is shown in Tables 6 and 7.

Table 6. Statistic metrics of models for Well A.

Models	R^2	RMSE	MAE	AAPE
Maurer (1962) [43]	−2.55	20.27	16.89	86.53
Bourgoyne and Young (1974) [36]	0.26	9.26	6.37	36.55
Al-Abduljabbar model (2018) [48]	−0.92	14.93	11.38	60.85
Proposed model with (DCM)	0.54	7.30	4.68	25.33

With Well A, a negative coefficient of determination ($R^2 = -2.55$) and the highest error rates (RMSE = 20.27, AAPE = 86.53%), the Maurer model (1962) completely contradicted the field data. This failure is attributed to the model's rigid reliance on *UCS*, which unfairly

penalizes ROP in harder regions. The Al-Abduljabbar model (2018) also produced a negative correlation (R^2 = −0.92) and an AAPE of 60.85%. The fixed exponents taken from a different domain were not appropriate for this well's unique lithology and drilling conditions, even though the model framework is robust.

Table 7. Statistic metrics of models for Well B.

Models	R^2	RMSE	MAE	AAPE
Maurer (1962) [43]	−2.2271	9.1083	7.5553	83.917
Bourgoyne and Young (1974) [36]	0.22282	4.6767	3.2764	57.989
Al-Abduljabbar model (2018) [48]	−1.4446	7.9276	6.3152	80.155
Proposed model with (DCM)	0.52151	3.5073	2.225	24.332

The Bourgoyne and Young model (1974) performed better than the fixed theoretical models, achieving a positive R^2 = 0.26 and reducing the AAPE to 36.55%. However, this accuracy is still insufficient for exact drilling optimization, emphasizing the necessity of a model that better captures geomechanics properties.

In order to improve prediction accuracy, the modified Al-Abduljabbar model examined sixteen separate geomechanics factors. The aim was to discover the parameter that better captures drillability than the widely used Unconfined Compressive Strength (*UCS*). Figure 10 lists the statistical ranking of the best predictors.

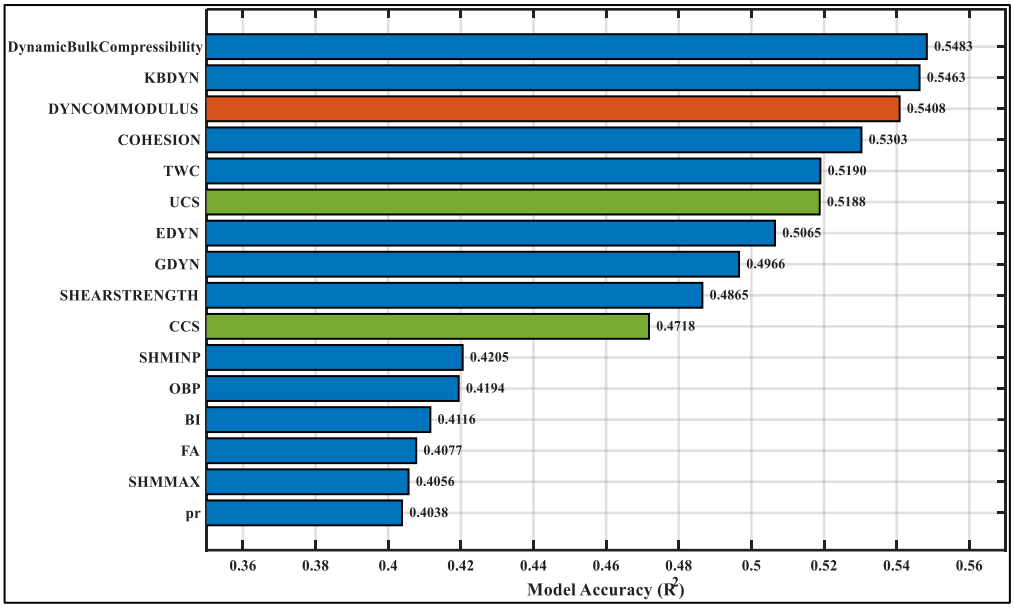

Figure 10. List of the statistical ranking of the best predictors.

The suggested modified Al-Abduljabbar model, which was optimized using multiple nonlinear regression and integrated with dynamic combined modulus (*DCM*), demonstrated superior predictive performance when compared to all compared models' baselines. The modified model achieved the highest accuracy, with (R^2 = 0.54), which doubled the explanatory power of the original Bourgoyne and Young model (R^2 = 0.26) and greatly outperformed the Maurer and original Al-Abduljabbar models, which had negative correlations. In addition to a 30% reduction in error compared to the Bourgoyne and Young model and a 70% reduction relative to the Maurer model, this increase in accuracy was coupled with a considerable decrease in error, with the revised model reaching the lowest RMSE = 7.30 and MAE = 4.68, giving the AAPE of 25.33%.

The natural heterogeneity of the drilled carbonate sequences—comprising limestone, dolomite, sandstone, shale, anhydrite, and marly limestone—is the primary explanation for the observed scatter and outliers in ROP predictions. Rapid vertical variations in lithology, porosity, fracture density, and diagenetic alteration produce localized departures between predicted and measured ROP that no single geomechanical parameter can fully capture. This variability is directly reflected in the wide standard deviations of the ROP data: Well A ranges from 1.9 to 92.7 m/hr (mean = 19.6, SD = 10.7 m/hr) and Well B from 1 to 43.8 m/hr (mean = 9.6, SD = 5.1 m/hr). In this context, the R^2 = 0.54 achieved by the DCM-modified model represents a practically meaningful result rather than a modeling deficiency.

Quantitative gains are visually confirmed by depth-based validation (Figures 11 and 12), where the modified model (green line) accurately replicates high-frequency ROP oscillations and drilling breaks that the baseline models, particularly the Maurer (red dash line) and original Al-Abduljabbar (blue dash line), were unable to capture. The modified method is now demonstrated to be the most trustworthy approach for predicting ROP in this sector because it can identify subtle variations in drillability that traditional drilling parameters alone cannot capture by incorporating the dynamic elastic response of the rock. Figure 13 show the cross plot of all models.

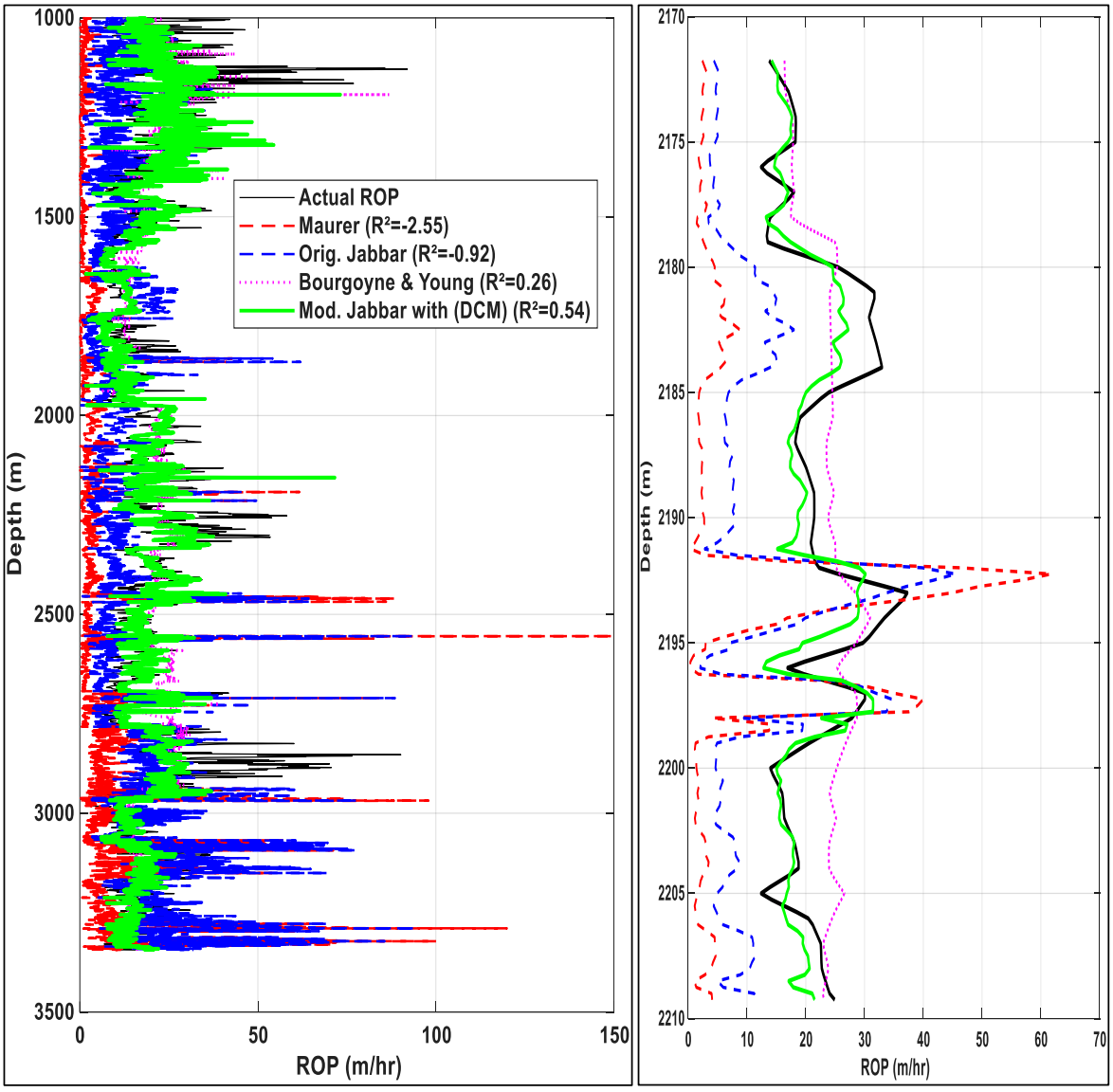

Figure 11. Comparison result of bast and modified ROP models for Well A.

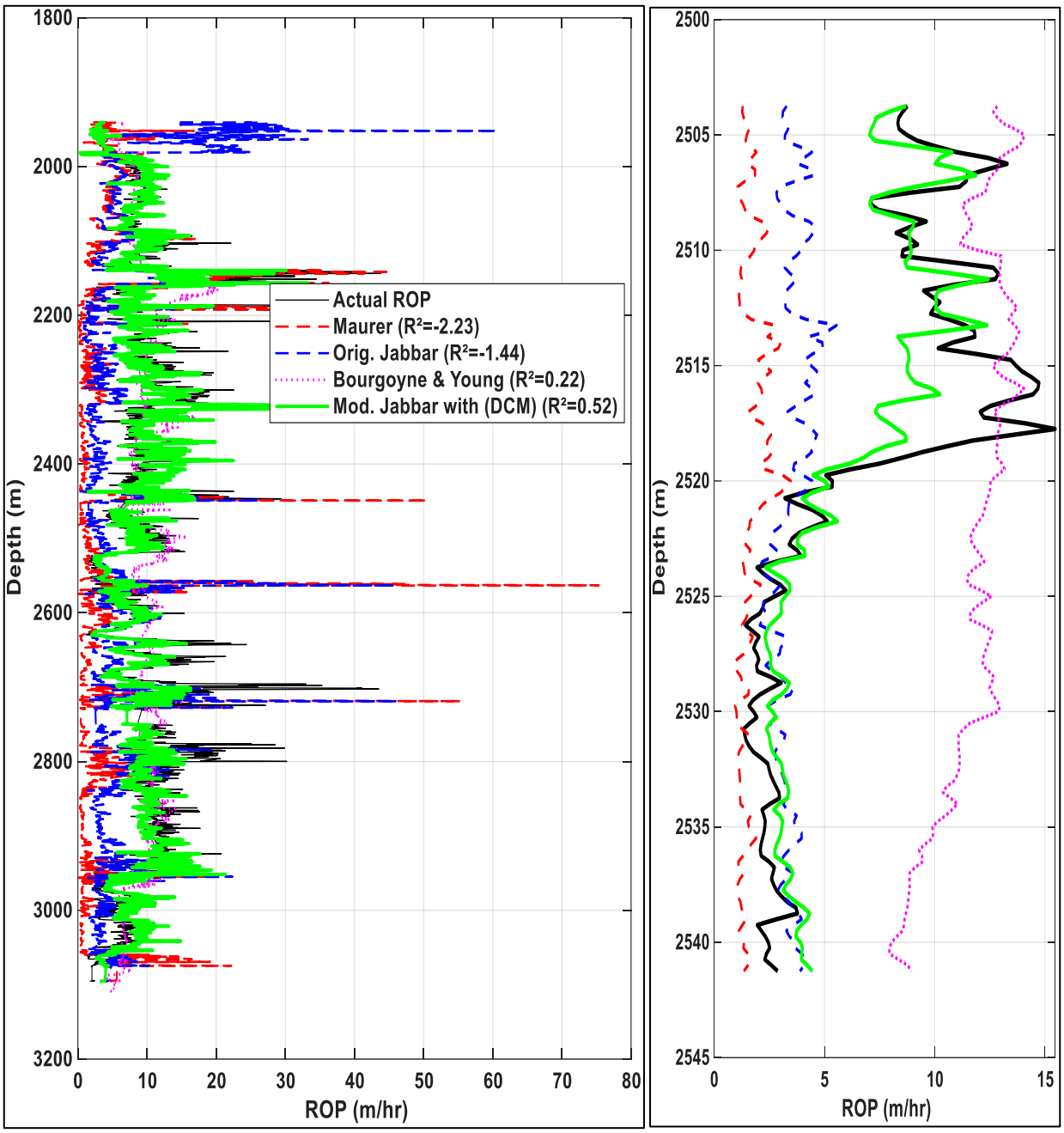

Figure 12. Comparison result of bast and modified ROP models for Well B.

While Dynamic Bulk Compressibility and K_{DYN} achieved the highest statistical accuracy (R^2 = 0.548), they face a critical operational limitation where both need Shear Sonic logs (DTSM) for computation. Shear sonic information is specialized and not always included in conventional drilling logging packages. On the other hand, dynamic combined modulus (*DCM*) produced a far better accuracy of (0.5408), which was about equal, compared to the industry-standard *UCS* (0.5188) and *CCS* (0.4718) while other parameters get accuracy with 0.40 such as (*pr*) which show the importance of select best geomechanics parameters. Importantly, the dynamic combined modulus (DCM) is determined using solely compressional sonic (DTCM) and density (RHOB) logs—common measurements found in practically all modern wells. However, other parameters, such as confined compressive strength (CCS) and shear strength (SS), require more information to be calculated, as they necessitate friction angle (j) and horizontal stress calculation. As a result, the dynamic combined modulus was chosen as the best predictor. It outperforms unconfined compressive strength

(UCS) by 4.2% in terms of variance explanation while remaining operationally viable for real-time applications.

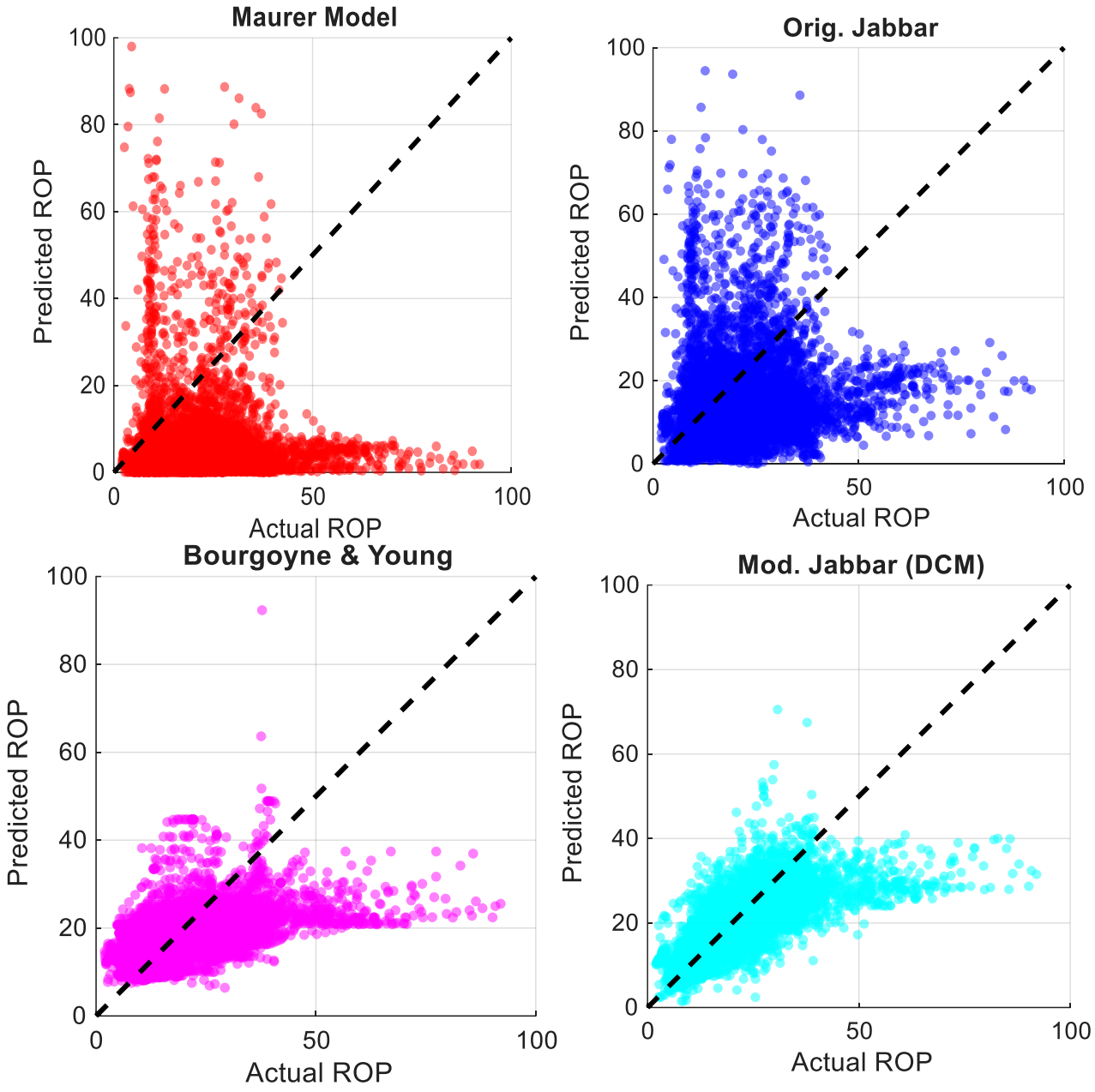

Figure 13. Cross plot between actual and predicted ROP through all model for Well A.

Equation (57) presents the final optimized equation for the studied field, considering the dynamic combined modulus (DCM). The regression analysis yielded particular exponents that reflect the physics of the drilling process.

$$ROP = 37.91 \frac{\left(RPM^{0.40} \times \rho^{2.71} \times TRQ^{1.2} \times HHP^{0.73}\right)}{\left(WOB^{-0.496} \times BS^{-3} \times \text{B}^{-3} \times \text{DCM}^{-0.498}\right)} \quad (57)$$

The actual relationship confirmed by the negative exponent for (*DCM*) is approximately (−0.50), which shows that the rate of penetration falls as the rock's stiffness (*DCM*) rises. Weight on bit has a negative exponent of −0.50, which suggests that it is more of a reactive operating practice than a physical constraint. Drillers instinctively increase *WOB* in

order to compensate for the increasing hardness of the formation and the natural decline of ROP. This creates a statistical artifact in the data set, where low ROP values are associated with high *WOB* values, which hides the theoretically advantageous correlation.

Mud weight results in a positive total exponent of (+2.72) because the positive correlation of the 8.5″ well section overcame the expected negative correlation seen in the 12.25″ well intervals resulting in unequal data distribution that skewed the parameter selection for the global model, where the longer 8.5″ well section statistically outperformed the shorter 12.25″ well section. Similarly, even though *CCS* was the superior predictor in the 12.25″ well size, the volume of data in the 8.5″ section is larger than 12.25″ well section, where *UCS* had a stronger correlation with ROP, and led to a higher overall accuracy for *UCS* (R^2 = 0.52) than *CCS* (R^2 = 0.47).

The depth-based predictions of the new dynamic combined modulus (*DCM*) model are compared against the *UCS* and *CCS* models in Figure 14. The dynamic combined modulus model (blue line) better captures the high-frequency variations in ROP than the UCS model (red dashed line) when there are rapid lithology changes. The statistical accuracy confirms the hierarchy: *DCM* (R^2 = 0.54); *CCS* (R^2 = 0.47); *UCS* (R^2 = 0.52). The dynamic elastic response of the rock shows that it is a better marker of drillability than fixed strength relationships based on its constant sonic and density log recording.

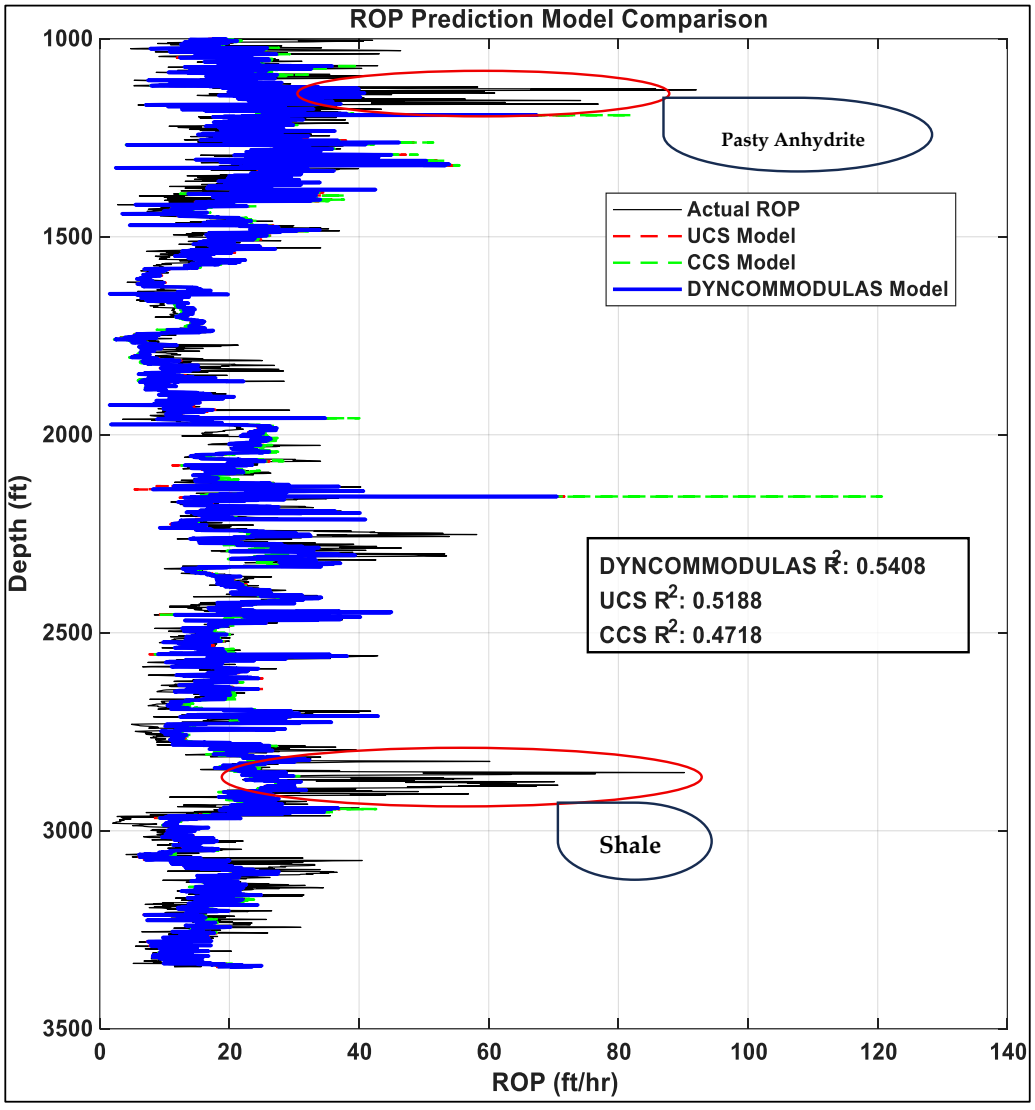

Figure 14. ROP model accuracy with different geomechanics parameters.

4. Conclusions

This study evaluated sixteen rock geomechanical properties to identify the most effective input for predicting drilling performance. The key findings of this study are as follows:

- Increasing rock strength reduces ROP, with shear strength and confined compressive strength (*CCS*) exhibiting the strongest negative correlations (Spearman = −0.68 and −0.67, respectively). Spearman correlations consistently exceeded Pearson values (e.g., shear strength: −0.68 vs. −0.52), demonstrating that the relationships are predominantly monotonic and nonlinear. This indicates that linear models are insufficient for accurate ROP forecasting, necessitating nonlinear or transformative approaches.
- Calculated results confirm that the in situ principal stresses and formation pore pressure significantly influence rock strength, indicating the importance of incorporating these factors in the geomechanical analysis for ROP prediction.
- The confined compressive strength (*CCS*) showed stronger correlation than unconfined compressive strength (*UCS*) for 12.25″ bits, while this relationship reversed for 8.5″ bits. This scale effect, attributed to bit–rock interaction volume, highlights that parameter selection for ROP models must include bit size.
- Dynamic bulk compressibility (BC_{DYN}) emerged as the strongest positive predictor of ROP (Pearson = 0.59, Spearman = 0.55), indicating that formations with greater compressibility facilitate more effective rock failure and higher penetration rates.
- The modified Al-Abduljabbar model calibrated using multiple nonlinear regression, significantly outperformed industry baselines (R^2 = 0.54 vs. R^2 < 0.26 for the Bourgoyne and Young model). Its superior performance stems from statistically optimizing exponents for local field conditions rather than relying solely on theoretical assumptions.
- Among all geomechanical properties evaluated, the dynamic combined modulus (*DCM*) was determined to be the most useful practical input. *DCM* generated strong correlations across all bit sizes and achieved the highest model accuracy (R^2 = 0.54) while requiring only conventional compressional sonic and density logs, offering a viable alternative to properties that depend on specialized shear sonic data.
- The contrast between *DCM* (R^2 = 0.54) and less relevant parameters such as friction angle (R^2 = 0.40) demonstrates that selecting the appropriate rock attribute is more consequential than mathematical coefficient tuning. This finding underscores that robust ROP modeling depends fundamentally on identifying the most physically relevant inputs.

Author Contributions: Conceptualization, M.A.K. and A.S.A.; methodology, M.A.K., M.N.J.A. and A.S.A.; software, M.A.K. and A.S.A.; validation, M.A.K.; formal analysis, M.A.K.; investigation, M.A.K.; resources, M.A.A.; data curation, M.A.K. and A.S.A.; writing—original draft preparation, M.A.K. and A.S.A.; writing—review and editing, M.A.K. and M.N.J.A.; visualization, M.A.K.; supervision, M.A.A. and F.S.A.; project administration, M.A.A. and F.S.A.; funding acquisition, M.A.A. All authors have read and agreed to the published version of the manuscript.

Funding: This research received no external funding.

Data Availability Statement: The original contributions presented in this study are included in the article. Further inquiries can be directed to the corresponding author.

Acknowledgments: This work was supported by the Ongoing Research Funding program, (ORF-2026-1422), King Saud University, Riyadh, Saudi Arabia. The authors would like to express their gratitude to the Department of Petroleum and Natural Gas Engineering at King Saud University for its assistance and support through this study.

Conflicts of Interest: The authors declare no conflicts of interest.

Nomenclature

Abbreviation/Symbol	Definition
BC_{DYN}	Dynamic bulk compressibility, μsip
BI	Brittleness index, fraction
BS	Bit size (bit diameter), in
c	Rock cohesion, psi
CCS	Confined compressive strength, psi
D	Depth, m
DCM	Dynamic combined modulus, Mpsi
DTCM	Compressional sonic log, μs/ft
DTSM	Shear sonic log, μs/ft
E_{DYN}	Dynamic Young's modulus, Mpsi
Est	Static Young's modulus, Mpsi
Fj	Jet impact force, lbf
FLOWPUMPS	Mud flow rate, l/min
G_{DYN}	Dynamic shear modulus, Mpsi
gp	Pore pressure gradient, ppg
GR	Gamma ray log, API
h	Bit tooth dullness, fraction
HHP	Hydraulic horsepower, hp
ISRM	International Society for Rock Mechanics and Rock Engineering
j	Internal friction angle (Mohr-Coulomb criterion), degree
K	Formation drillability constant
K_{DYN}	Dynamic bulk modulus, Mpsi
MW	Mud weight, g/cc (field data; Well logs, Tables 2–5)
MWin	Mud weight in (flow-in), g/cc
MWout	Mud weight out (return), g/cc
NCTL	Normal Compaction Trend Line
NPHI	Neutron porosity, fraction
OBP	Overburden pressure, psi
PDC	Polycrystalline Diamond Compact (bit type)
PEF	Photoelectric factor log
Φ	Porosity, fraction
PP	Pore pressure, psi
PPn	Normal hydrostatic pressure, psi
pr	Dynamic Poisson's ratio, fraction
PV	Plastic viscosity, cp
Q	Flow rate, gpm
RD	Deep resistivity log, ohm·m (API standard)
RHOB	Density log, g/cc
ROP	Rate of penetration, m/hr
RPM	Rotary speed, revolutions per minute
SHMMAX	Maximum horizontal stress, psi
SHMINP	Minimum horizontal stress, psi
SP	Spontaneous potential log, mV
SPP	Standpipe pressure, psi
SS	Shear strength, psi
TEMP	Formation temperature log, °C
TNPH	Thermal neutron porosity log, fraction
TRQ	Torque, klbf·ft
TVD	True vertical depth, m
TWC	Thick-walled cylinder strength, psi
UCS	Unconfined compressive strength, psi

Vclay	Clay volume fraction
WOB	Weight on bit, ton (field data); lbf (model equations)
$(WOB/BS)_t$	Threshold bit weight per inch of bit diameter, psi
Δt_{NCT}	Acoustic travel time from the Normal Compaction Trend Line at depth, μs/ft
$\Delta t_{observed}$	Acoustic travel time measured from sonic log, μs/ft
ρ	Mud density, pcf—used in Al-Abduljabbar model (Equation (55)) only; see MW for field data units
σ_n	Normal effective stress, psi

References

1. Messaoud, L. Influence of fluids on the essential parameters of rotary percussive drilling. *Lab. Environ.* **2009**, *14*, 1–8.
2. Munoz, H.; Taheri, A.; Chanda, E.K. Rock Drilling Performance Evaluation by an Energy Dissipation Based Rock Brittleness Index. *Rock Mech. Rock Eng.* **2016**, *49*, 3343–3355. [CrossRef]
3. Paone, J.; Madson, D.; Bruce, W.E. *Drillability Studies-Laboratory Percussive Drilling*; US Department of the Interior, Bureau of Mines: Washington, CD, USA, 1969.
4. Tandanand, S.; Unger, H.F. *Drillability Determination: A Drillability Index for Percussion Drills*; US Department of the Interior, Bureau of Mines: Washington, CD, USA, 1975; Volume 8073.
5. Perrin, V.P.; Mensa-Wilmot, G.; Alexander, W.L. Drilling Index—A New Approach to Bit Performance Evaluation. In Proceedings of the SPE/IADC Drilling Conference, Amsterdam, The Netherlands, 4–6 March 1997; p. SPE-37595-MS.
6. Cheniany, A.; Hasan, K.S.; Shahriar, K.; Khademi Hamidi, J. An estimation of the penetration rate of rotary drills using the Specific Rock Mass Drillability index. *Int. J. Min. Sci. Technol.* **2012**, *22*, 187–193. [CrossRef]
7. Bilim, N. Determination of drillability of some natural stones and their association with rock properties. *Sci. Res. Essays* **2011**, *6*, 382–387.
8. Copur, H.; Cinar, M.; Okten, G.; Bilgin, N. A case study on the methane explosion in the excavation chamber of an EPB-TBM and lessons learnt including some recent accidents. *Tunn. Undergr. Space Technol.* **2012**, *27*, 159–167. [CrossRef]
9. Plumb, R.; Edwards, S.; Pidcock, G.; Lee, D.; Stacey, B. The Mechanical Earth Model Concept and Its Application to High-Risk Well Construction Projects. In Proceedings of the IADC/SPE Drilling Conference, New Orleans, LA, USA, 23–25 February 2000; p. SPE-59128-MS.
10. Zoback, M.D. *Reservoir Geomechanics*; Cambridge University Press: Cambridge, UK, 2010.
11. Xu, H.; Zhou, W.; Xie, R.; Da, L.; Xiao, C.; Shan, Y.; Zhang, H. Characterization of Rock Mechanical Properties Using Lab Tests and Numerical Interpretation Model of Well Logs. *Math. Probl. Eng.* **2016**, *2016*, 5967159. [CrossRef]
12. Kahraman, S.; Bilgin, N.; Feridunoglu, C. Dominant rock properties affecting the penetration rate of percussive drills. *Int. J. Rock Mech. Min. Sci.* **2003**, *40*, 711–723. [CrossRef]
13. Yenice, H. Determination of drilling rate index based on rock strength using regression analysis. *An. Acad. Bras. Ciênc.* **2019**, *91*, e20181095. [CrossRef]
14. Cunningham, R.A. An Empirical Approach For Relating Drilling Parameters. *J. Pet. Technol.* **1978**, *30*, 987–991. [CrossRef]
15. Walker, B.H.; Black, A.D.; Klauber, W.P.; Little, T.; Khodaverdian, M. Roller-Bit Penetration Rate Response as a Function of Rock Properties and Well Depth. In Proceedings of the SPE Annual Technical Conference and Exhibition, New Orleans, LA, USA, 5–8 October 1986; p. SPE-15620-MS.
16. Warren, T.M. Drilling Model for Soft-Formation Bits. *J. Pet. Technol.* **1981**, *33*, 963–970. [CrossRef]
17. Warren, T.M. Factors Affecting Torque for a Roller Cone Bit. *J. Pet. Technol.* **1984**, *36*, 1500–1508. [CrossRef]
18. Delavar, M.R.; Ramezanzadeh, A.; Tokhmechi, B. An investigation into the effect of geomechanical properties of reservoir rock on drilling parameters—A case study. *Arab. J. Geosci.* **2021**, *14*, 1763. [CrossRef]
19. Al-Betairi, E.A.; Moussa, M.M.; Al-Otaibi, S. Multiple Regression Approach To Optimize Drilling Operations in the Arabian Gulf Area. *SPE Drill. Eng.* **1988**, *3*, 83–88. [CrossRef]
20. Hareland, G.; Hoberock, L.L. Use of Drilling Parameters to Predict In-Situ Stress Bounds. In Proceedings of the SPE/IADC Drilling Conference, Amsterdam, The Netherlands, 22–25 February 1993; p. SPE-25727-MS.
21. Pandey, A.; Jain, A.; Singh, D. An investigation into rock drilling. *Int. J. Surf. Min. Reclam. Environ.* **1991**, *5*, 135–141. [CrossRef]
22. Altindag, R. The evaluation of rock brittleness concept on rotary blast hold drills. *J. South. Afr. Inst. Min. Metall.* **2002**, *102*, 61–66.
23. Bilgin, N.; Kahraman, S. Drillability prediction in rotary blast hole drilling. In Proceedings of the 18th International Mining Congress and Exhibition of Turkey, Antalya, Turkey, 10–13 June 2003; pp. 177–182.

24. Judzis, A.; Bland, R.G.; Curry, D.A.; Black, A.D.; Robertson, H.A.; Meiners, M.J.; Grant, T.C. Optimization of Deep-Drilling Performance—Benchmark Testing Drives ROP Improvements for Bits and Drilling Fluids. *SPE Drill. Complet.* **2009**, *24*, 25–39. [CrossRef]
25. Yenice, H.; Özfirat, M.; Karaca, Z.; Kahraman, B. Investigation of the parameters effecting Drilling Rate Index (DRI) of Marbles. In Proceedings of the 2nd Mining Machinery Symposium of Turkey, Zonguldak, Turkey, 4–6 November 2009; pp. 4–6.
26. Prasad, U. Drillability of a Rock In Terms of Its Physico-Mechanical And Micro-Structural Properties. In Proceedings of the 43rd U.S. Rock Mechanics Symposium & 4th U.S.-Canada Rock Mechanics Symposium, Asheville, NC, USA, 28 June–1 July 2009; p. ARMA-09-040.
27. Yaşar, E.; Ranjith, P.G.; Viete, D.R. An experimental investigation into the drilling and physico-mechanical properties of a rock-like brittle material. *J. Pet. Sci. Eng.* **2011**, *76*, 185–193. [CrossRef]
28. Yarali, O.; Soyer, E. Assessment of relationships between drilling rate index and mechanical properties of rocks. *Tunn. Undergr. Space Technol.* **2013**, *33*, 46–53. [CrossRef]
29. Li, G.; Yang, M.; Meng, Y.; Liu, H.; Han, L.; Zhou, F.; Zhang, H. The assessment of correlation between rock drillability and mechanical properties in the laboratory and in the field under different pressure conditions. *J. Nat. Gas Sci. Eng.* **2016**, *30*, 405–413. [CrossRef]
30. Li, W.; Ling, X.; Pu, H. Development of a Cutting Force Model for a Single PDC Cutter Based on the Rock Stress State. *Rock Mech. Rock Eng.* **2020**, *53*, 185–200. [CrossRef]
31. Kolapo, P. Investigating the Effects of Mechanical Properties of Rocks on Specific Energy and Penetration Rate of Borehole Drilling. *Geotech. Geol. Eng.* **2021**, *39*, 1715–1726. [CrossRef]
32. Graham, J.W.; Muench, N.L. Analytical Determination of Optimum Bit Weight and Rotary Speed Combinations. In Proceedings of the Fall Meeting of the Society of Petroleum Engineers of AIME, Dallas, TX, USA, 4–7 October 1959; p. SPE-1349-G.
33. Galle, E.; Woods, H. *Best Constant Weight and Potary Speed for Rotary Rock Bits*; Hughes Tool Company: Houston, TX, USA, 1963.
34. Bingham, M.G. *A New Approach to Interpreting—Rock Drillability*; Petroleum Pub. Co.: Tulsa, OK, USA, 1965.
35. Eckel, J.R. Microbit Studies of the Effect of Fluid Properties And Hydraulics on Drilling Rate, II. In Proceedings of the Fall Meeting of the Society of Petroleum Engineers of AIME, Houston, TX, USA, 29 September–2 October 1968; p. SPE-2244-MS.
36. Bourgoyne, A.T., Jr.; Young, F.S., Jr. A Multiple Regression Approach to Optimal Drilling and Abnormal Pressure Detection. *Soc. Pet. Eng. J.* **1974**, *14*, 371–384. [CrossRef]
37. Jahanbakhshi, R.; Keshavarzi, R.; Jafarnezhad, A. Real-time Prediction of Rate of Penetration During Drilling Operation In Oil And Gas Wells. In Proceedings of the 46th U.S. Rock Mechanics/Geomechanics Symposium, Chicago, IL, USA, 24–27 June 2012; p. ARMA-2012-2244.
38. Ahmed, O.S.; Adeniran, A.A.; Samsuri, A. Computational intelligence based prediction of drilling rate of penetration: A comparative study. *J. Pet. Sci. Eng.* **2019**, *172*, 1–12. [CrossRef]
39. Lawal, A.I.; Kwon, S.; Onifade, M. Prediction of rock penetration rate using a novel antlion optimized ANN and statistical modelling. *J. Afr. Earth Sci.* **2021**, *182*, 104287. [CrossRef]
40. Shaker, T.J.; Hadi, F.A. Development of Artificial Intelligence Models for Estimating Rate of Penetration in East Baghdad Field, Middle Iraq. *Iraqi Geol. J.* **2022**, *55*, 112–124. [CrossRef]
41. Jiao, S.; Li, W.; Li, Z.; Gai, J.; Zou, L.; Su, Y. Hybrid physics-machine learning models for predicting rate of penetration in the Halahatang oil field, Tarim Basin. *Sci. Rep.* **2024**, *14*, 5957. [CrossRef]
42. Huang, G.; Hamzah, S.K.; Patel, P.; Ramachandran, T.; Shankhyan, A.; Karthikeyan, A.; Thatoi, D.N.; Gupta, D.; AbdulAmeer, S.; Alwan, M.; et al. Data-driven prediction of rate of penetration (ROP) in drilling operations using advanced machine learning models. *J. Pet. Explor. Prod. Technol.* **2025**, *15*, 121. [CrossRef]
43. Maurer, W.C. The "Perfect-Cleaning" Theory of Rotary Drilling. *J. Pet. Technol.* **1962**, *14*, 1270–1274. [CrossRef]
44. Hareland, G.; Rampersad, P.R. Drag-Bit Model Including Wear. In Proceedings of the SPE Latin America/Caribbean Petroleum Engineering Conference, Buenos Aires, Argentina, 27–29 April 1994; p. SPE-26957-MS.
45. Warren, T.M. Penetration-Rate Performance of Roller-Cone Bits. *SPE Drill. Eng.* **1987**, *2*, 9–18. [CrossRef]
46. Deng, Y.; Chen, M.; Jin, Y.; Zhang, Y.; Zou, D.; Lu, Y. Theoretical and experimental study on the penetration rate for roller cone bits based on the rock dynamic strength and drilling parameters. *J. Nat. Gas Sci. Eng.* **2016**, *36*, 117–123. [CrossRef]
47. Motahhari, H.R.; Hareland, G.; James, J.A. Improved Drilling Efficiency Technique Using Integrated PDM and PDC Bit Parameters. *J. Can. Pet. Technol.* **2010**, *49*, 45–52. [CrossRef]
48. Al-AbdulJabbar, A.; Elkatatny, S.; Mahmoud, M.; Abdelgawad, K.; Al-Majed, A. A Robust Rate of Penetration Model for Carbonate Formation. *J. Energy Resour. Technol.* **2018**, *141*, 042903. [CrossRef]
49. Mohammadi Behboud, M.; Ramezanzadeh, A.; Tokhmechi, B.; Mehrad, M.; Davoodi, S. Estimation of geomechanical rock characteristics from specific energy data using combination of wavelet transform with ANFIS-PSO algorithm. *J. Pet. Explor. Prod. Technol.* **2023**, *13*, 1715–1740. [CrossRef]

50. Delavar, M.R.; Ramezanzadeh, A. Machine learning classification approaches to optimize ROP and TOB using drilling and geomechanical parameters in a carbonate reservoir. *J. Pet. Explor. Prod. Technol.* **2024**, *14*, 1–26. [CrossRef]
51. Saad, A.; Taman, A.; Reda, D.; Yehia, T.; Keshinro, O.; Meehan, N.; Okoroafor, E.R. Enhancing Geothermal Drilling Performance: Predicting Rate of Penetration with Machine Learning Utilizing Geomechanical and Petrophysical Data. In Proceedings of the SPE Offshore Europe Conference & Exhibition, Scotland, UK, 2–5 September 2025.
52. Rickman, R.; Mullen, M.; Petre, E.; Grieser, B.; Kundert, D. A Practical Use of Shale Petrophysics for Stimulation Design Optimization: All Shale Plays Are Not Clones of the Barnett Shale. In Proceedings of the SPE Annual Technical Conference and Exhibition, Moscow, Russia, 28–30 October 2008.
53. Eaton, B.A. Fracture Gradient Prediction and Its Application in Oilfield Operations. *J. Pet. Technol.* **1969**, *21*, 1353–1360. [CrossRef]
54. Li, S.; Purdy, C. Maximum Horizontal Stress and Wellbore Stability While Drilling: Modeling and Case Study. In Proceedings of the SPE Latin American and Caribbean Petroleum Engineering Conference, Lima, Peru, 1–3 December 2010.